J. Membrane Biol. 14, 243–292 (1973)
© by Springer-Verlag New York Inc. 1973

Slow Conductance Changes due to Potassium Depletion in the Transverse Tubules of Frog Muscle Fibers during Hyperpolarizing Pulses

Peter H. Barry* and Richard H. Adrian
(with appendices by Peter H. Barry)

Physiological Laboratory, University of Cambridge, England

Received 7 June 1973

Summary. When hyperpolarizing currents are applied between the inside and outside of a muscle fiber it is known that there is a slow transient decrease (300- to 600-msec time constant) in the measured fiber conductance sometimes referred to as "creep" which is maximal in K_2SO_4 Ringer's solutions and which disappears on disruption of the transverse tubular system. An approximate mathematical analysis of the situation indicates that these large, slow conductance changes are to be expected from changes in the K^+ concentration in the tubular system and are due to differences in transport numbers between the walls and lumen of the tubules. Experiments using small constant-voltage and constant-current pulses (membrane p. d. changes $\lesssim$20 to 30 mV) on the same fibers followed by an approximate mathematical and more exact computed numerical analysis using the measured fiber parameters and published values of tubular system geometry factors showed close agreement between the conductance creep predicted and that observed, thus dispensing with the need for postulated changes in individual membrane conductances at least during small voltage pulses. It is further suggested that an examination of creep with constant-voltage and constant-current pulses may provide a useful tool for monitoring changes in tubular system parameters, such as those occurring during its disruption by presoaking the fibers in glycerol.

Table of Main Symbols Used

R, T, F	Gas constant, Temperature in °K and the Faraday
a	Fiber radius
r	Radial distance from the center of the fiber (*cf.* Fig. 2*A*)
t	Time in sec
V_1, V_2	Voltages measured by electrodes 1 and 2 (*cf.* p. 248)
λ	Longitudinal fiber space constant ($\lambda^2 = R_m a/2R_i$)
$R_m, R_m(t)$	Total membrane resistance per unit surface area of fiber (Ω cm^2)

* *Present address*: School of Physiology and Pharmacology, University of New South Wales, Australia.

$R_m(0)$, $R_m(\infty)$	As above at $t=0$ (excluding capacity transient) and at $t=\infty$ during a current or voltage pulse
G_m, $G_m(t)$	Total membrane conductance (mho·cm^{-2}) per unit area of fiber surface
$G_m(0)$, $G_m(\infty)$	As above at $t=0$ (excluding the capacity transient) and at $t=\infty$ during a current or voltage pulse
R_{sm}, G_{sm}	Surface membrane resistance (Ω cm^2) and conductance (mho·cm^{-2}), respectively, excluding the TTS
R_T, G_T	Input resistance (Ω cm^2) and conductance (mho·cm^{-2}) of the TTS referred to unit area of fiber surface
f_T	Fraction of the K^+ conductance in the TTS to the total K^+ conductance of the fiber [*cf.* Eq. (7)]
R_i	Internal resistivity of the fiber (Ω cm)
r_s	Electrical access resistance of the TTS [Ω cm^2; *cf.* Fig. 3 and Eq. (24)]
h	Diffusional access resistance of the TTS [*cf.* Eq. (27)]
I_0	Total current entering fiber (amp)
I_m, i_m	Total current per unit area of fiber surface (amp·cm^{-2}; considered positive in the hyperpolarizing direction)
i_{sm}	Current going through the surface membrane alone (amp·cm^{-2}; *cf.* Fig. 3)
i_0, $i_0(t)$	Total current entering the TTS referred to unit area of surface membrane (amp·cm^{-2}; *cf.* Fig. 3)
I_K, $I_K(r)$	K^+ current density crossing the equivalent TTS disc at radial distance r [*cf.* Fig. 2*A* and Eq. (23)]
i, $i(r, t)$	Radial current in the lumen of the TTS at radial distance r and time t (*cf.* Fig. 2*B*)
C, $C(r, t)$	K^+ concentration within the TTS at radial distance r and time t (mEquiv·liter^{-1})
C_o, C_K	Both refer to external solution and initial TTS K^+ concentration (mEquiv·liter^{-1})
V, $V(r, t)$	The potential at radial distance r in the lumen of the TTS with respect to the external solution at time t (*cf.* Figs. 2 and 3)
$V(a)$, $V(a, t)$	The p.d. across the access resistance (*cf.* Figs. 3*B* and 3*C*)
V_0, $V_0(t)$	The potential of the sarcoplasm with respect to the external solution (*cf.* Figs. 2 and 3)
E_K	The K^+ equilibrium potential between the sarcoplasm and the externa solution or across the tubular wall
t_K^m, t_K^s	The transport number for K^+ in the TTS membranes and in the solution of the tubular lumen, respectively
ρ	The fraction of fiber volume occupied by tubules, and not implicitly including branches
ρ'	As above but always including branches
σ	A dimensionless network factor for the TTS
G_W	Conductance per unit area of tubular wall (mho·cm^{-2})
G_L	Conductance of tubular lumen (mho·cm^{-1})
ξ	Volume-to-surface ratio of the TTS

$\bar{G}_W$	Effective wall conductance of TTS membranes per unit volume of fiber [mho·cm^{-3}; *cf.* Eq. (14)]
$\bar{G}_L$	Effective radial conductance of the lumen of the TTS per unit volume of fiber [*cf.* Eq. (20)]
d	The thickness of the equivalent disc representing the TTS [*cf.* Eq. (15)]
λ_T	Space constant of the TTS [*cf.* Eq. (37). *cp.* Eq. (11)]
D_K	The diffusion coefficient of K^+ ions in the lumen of the TTS (cm^2 sec^{-1})
$\bar{D}_K$	The effective radial K^+ diffusion coefficient in the TTS [*cf.* Eq. (28)]
J_0, J_1	Bessel functions of order "0" and "1", respectively
I_0, I_1	Modified Bessel functions of order "0" and "1", respectively
τ	Time constants of slow conductance changes
τ_{vc}	Time constant of slow conductance changes during a constant-voltage pulse
τ_{cc}	Time constant of slow conductance changes during a constant-current pulse
α, α_m	Roots of various Bessel function equations
g_1, g_2, g_3, g_4	Constants used to fit cubic equation for conductance-voltage curves [*cf.* Eq. (71)]

It has been known for a long time (Schaefer, Schölmerich & Haass, 1939; Katz, 1949) that when hyperpolarizing currents are applied between the inside and the outside of a muscle fiber there are slow time-dependent changes in the current or voltage traces corresponding to a decrease in the measured membrane conductance of that fiber. Adrian and Freygang (1962) suggested that this could possibly be due to changes in the concentrations of K^+ in the transverse tubules of the muscle fiber. They further showed that this "conductance creep" phenomenon only seemed to occur when K^+ was in the bathing solution and that it was accentuated when a fairly impermeable anion such as SO_4^{2-} replaced Cl^- in the bathing solution. This they had suggested could result from the transverse tubular system, henceforth referred to as the "TTS", behaving as the central compartment of a three-compartment system: one membrane would be equivalent to that between the tubular lumen and the sarcoplasm with a voltage-dependent permeability and only permeable to K^+, and the other membrane would be a hypothetical one postulated as being between the tubular lumen and the external solution and having a constant permeability to both sodium and potassium. In double pulse experiments they found that the first pulse tended to precondition the fiber for the second pulse as expected from such a hypothesis. Their model seemed to agree reasonably well qualitatively with their experimental results.

Since then Gage and Eisenberg (1969) have shown that when the TTS is disconnected from the surface membrane by pre-soaking the muscle fibers in a glycerol Ringer's solution this conductance creep phenomenon disappeared, thus confirming that the TTS was involved in the mechanism.

Also, Endo (1966), Huxley (1964) and Page (1964) have shown that the transverse tubules are quite open to the diffusion of even large molecules like Lissamine Rhodamine B200 (mol wt = 558) or Ferritin, thus destroying the assumption of a second selective membrane at the mouth of the tubules. Adrian, Chandler and Hodgkin (1970*b*), however, pointed out that this does not negate the Adrian-Freygang hypothesis completely since K^+ should have different transport numbers in the lumen and wall of the TTS. However, in their paper they seriously question how much of this conductance creep effect would be explained by the hypothesis. In particular, some of their experiments at hyperpolarizations to -150 mV in 2.5 mM K sulfate Ringer's solution seemed difficult to reconcile with a simple K^+ depletion model. For example, current-voltage relationships at the end of similar large constant-voltage pulses showed a negative slope, something not expected from the Adrian-Freygang hypothesis alone. In addition, attempts to measure the equilibrium potential at the end of such large constant-voltage pulses seemed to indicate virtually no change in it. This certainly was unexpected at the time since in general a change in K^+ ion concentration, on one side of a membrane if it is the principal permeating species, should normally be reflected in a change in equilibrium potential.

Very recently, Almers (1972*a*, *b*) has carried out a further investigation of these slow conductance changes and has successfully met these two main objections against the K^+ depletion hypothesis. First of all, Almers (1972*a*) correctly points out that because of inward rectification in the transverse tubules, at the termination of a current pulse after which K^+ current flows in the high resistance direction, any change in the K^+ equilibrium potential across the tubular walls will be very effectively shunted out by the lower surface membrane resistance. He predicted that there should nevertheless be small changes in the total K^+ equilibrium potential between the sarcoplasm and external solution of the fiber, and in some two- and three-electrode experiments has measured changes of between 2 and 4 mV. These are of the order expected and are in the direction consistent with a lowering of the K^+ concentration in the TTS. Secondly, in some elegant experiments he shows that these slow changes in membrane conductance can be divided into two components. For changes *to* membrane potentials less negative than about -120 mV there is a component which has a slow recovery after the pulse with a Q_{10} of about 1.3 as expected from a diffusion limited process. At

more negative voltages, Almers (1972*b*) shows that there is in addition a component with a much faster recovery and which has a Q_{10} of 3.0 for the rate of conductance decline and 2.8 for the rate of subsequent recovery after the pulse. As he points out these two high Q_{10}'s are of the same order as those found for the kinetics of permeability changes in nerve action potentials and strongly suggest that this component is a time- and voltage-dependent membrane permeability change. He was able to separate the effects of these two components at the higher voltages and show that the region of negative slope in the current-voltage curves was a property of this latter component alone.

In addition, he showed in a series of two-pulse voltage-clamp experiments that the recovery of the current following a voltage pulse could satisfactorily be reconstructed from conductance-concentration curves on the basis of reduced K^+ concentrations in the transverse tubules at the lower membrane potentials.

Finally, he showed that at these lower potentials the extent of conductance decline, steady-state current, and initial rate of recovery were consistent with the depletion hypothesis.

To further confirm that depletion of K^+ provides an adequate explanation for these lower voltage slow conductance changes, this paper seeks to look at the problem from the opposite point of view and ask the question "What mechanism would be expected on physico-chemical grounds?". As Adrian *et al.* (1970*b*) recognized, electrical currents must in general produce changes in local ion concentrations whenever there are transport number differences between membranes and adjacent solutions (e.g. Barry & Hope, 1969*a*, *b*; Wedner & Diamond, 1969; *see also* Dewhurst, 1960), the transport number of an ion representing the fraction of current carried by that ion. In fact, similar slow transient changes in measured input resistance (voltage/current) were seen across the cylindrical membranes of giant algal cells (Barry & Hope, 1969*b*) and even across planar segments of algal cell walls, which behave as cation-exchange resins. These were shown to be caused by local enhancement and depletion of the salt concentration in the unstirred regions adjacent to cell membranes due to transport number differences and in fact even caused local osmotic water flows at first mistaken for electro-osmosis.

Thus, approaching the problem from this direction the more specific question which this paper will seek to answer becomes: "Given the present knowledge of the geometry of the tubular system and the appropriate electrical parameters of muscle fibers, what will be the magnitudes of such transport number effects, in what detailed ways will they manifest themselves

and will they completely explain the experimental observations?". To answer this question, a theoretical analysis of these transport number effects in the TTS of a muscle fiber was undertaken, using a distributed model for the TTS similar to that proposed by Adrian, Chandler and Hodgkin (1969). This model initially involved an approximate mathematical analysis based on the assumption that the K^+ conductance was constant and independent of the membrane potential. Such an analysis predicted, for example, that there should be symmetry between the time-course of the current during a constant-voltage pulse and its subsequent reversal at the end of the applied pulse. However, experimentally there is considerable asymmetry between the two time-courses, but then it is also well known that conductance is very dependent on driving force since the tubular membrane acts as an inward rectifier for K^+. To take into account this nonlinear relationship between conductance and driving force it was necessary to undertake a more exact numerical analysis by computer. Both analyses indicated that there should be significant changes in the concentration of K^+ in the transverse tubules of muscle fibers and slow time-dependent conductance changes of the same order of magnitude and time-course as had been observed previously (Adrian & Freygang, 1962; Adrian *et al.*, 1970*b*; Almers, 1972*a*, *b*). Similarly, the numerical analysis does predict the sort of asymmetry measured experimentally. This paper then describes a series of experiments under conditions of constant voltage and constant current. The basic membrane parameters for each fiber were then measured and taking the generally accepted values of the TTS parameters, a comparison was made of the experimentally measured slow conductance changes in these fibers against those predicted theoretically.

In addition, such theoretical analyses provide insight into the mechanism of K^+ depletion in the TTS and predict further experiments that may be undertaken. They also suggest, for example, that an examination of the time-courses of such slow conductance changes with constant-current and constant-voltage pulses may provide a useful tool for monitoring changes in tubular system parameters.

Methods

The technique for measuring membrane parameters and for monitoring the resistance creep was the three-electrode technique. It was essentially the same as that used by Adrian, Chandler and Hodgkin (1970*a*), and will only be described briefly. Three electrodes were inserted at distances l, $2l$ and $2l+l'$ from the pelvic end of a fiber in the sartorius muscle of *Rana temporaria*. The spacing employed was 0.5, 1.0 and 1.1 mm and clamping control was taken from the potential at the middle electrode (V_2, where $x=2l$) instead of the potential at the end electrode (V_1, where $x=l$) which they normally used. Short,

constant-voltage pulses of about 100-msec duration were used to measure the fiber parameters. The space constant of the fiber λ was obtained numerically from the exact equation (*cf.* Adrian *et al.*, 1970*a*):

$$\frac{\mathrm{Cosh}\,(2l/\lambda)}{\mathrm{Cosh}\,(l/\lambda)}=\left(\frac{V_2-V_1}{V_1}\right)+1 \tag{1}$$

rather than the more approximate one:

$$\frac{V_2-V_1}{V_1}\approx\frac{3}{2}(l/\lambda)^2. \tag{2}$$

The resistance per unit length of the fiber r_i was calculated from the equation:

$$r_i=\frac{V_1(\mathrm{Cosh}\,(2l+l')/\lambda+\mathrm{Sinh}\,(2l+l')/\lambda)}{I_0\lambda\,\mathrm{Cosh}\,(l/\lambda)} \tag{3}$$

where I_0 is the current applied by the third electrode at $x=2l+l'$.

The fiber radius a and the membrane current per unit area of fiber surface I_m were then calculated from the equations (Adrian *et al.*, 1970*a*):

$$a=\sqrt{R_i/\pi r_i} \tag{4}$$

and

$$I_m(l)=\frac{a(V_2-V_1)\,\mathrm{Cosh}\,(l/\lambda)}{2R_i\lambda^2\left[\mathrm{Cosh}\left(\frac{2l}{\lambda}\right)-\mathrm{Cosh}\left(\frac{l}{\lambda}\right)\right]} \tag{5}$$

where R_i, the internal resistivity of the fiber, was assumed to have the value obtained by Nakajima and Hodgkin (1970), i.e. 169 Ω cm at 20 °C.

The measured membrane resistance per unit area R_m (actually the resistance of the surface membrane and TTS in parallel) is given (Adrian *et al.*, 1970*a*) by:

$$R_m=V_1/I_m. \tag{6}$$

If the fraction f_T of K^+ conductance in the TTS to total K^+ conductance is known, then the conductance of the TTS, G_T, and the resistance of the surface membrane R_{sm} of the muscle fiber can be obtained from the total membrane resistance R_m by:

$$G_T=f_T/R_m \tag{7}$$

and similarly

$$R_{sm}=R_m/(1-f_T). \tag{8}$$

Following Adrian *et al.* (1969), although now adding an access resistance term r_s for the TTS, it may be simply shown that the effective wall conductance $\bar{G}_W$ is given by the approximate equation:

$$\bar{G}_W\approx 2\Big/\left[a\left(\frac{1}{G_T}-\frac{a}{4\bar{G}_L}-r_s\right)\right]. \tag{9}$$

The actual full equation for the TTS conductance for a muscle fiber with an access resistance will be published later and may be shown to be given by:

$$G_T = \frac{\bar{G}_W \lambda_T I_1(a/\lambda_T)}{I_0(a/\lambda_T) + \frac{r_s \bar{G}_L}{\lambda_T} I_1(a/\lambda_T)} \tag{10}$$

where

$$\lambda_T = \sqrt{\bar{G}_L/\bar{G}_W} \tag{11}$$

where $I_0(a/\lambda_T)$ and $I_1(a/\lambda_T)$ are the tabulated or easily calculable modified Bessel functions of order "0" and "1", respectively (e.g., Abramowitz & Stegun, 1965) and where $\bar{G}_L$ is the effective conductance of the lumen of the transverse tubules. Eqs. (10) and (11) may be solved numerically for $\bar{G}_W$. Although Eq. (9) is in fact reasonably accurate (error$\lesssim$0.1 % for typical fiber parameters), Eqs. (10) and (11) were used in practice.

Thus, $\bar{G}_W$ and R_{sm} can be estimated from the ratios of R_m, a and f_T. Eisenberg and Gage (1969) measured a value of 0.66 [i.e. 55/(55+28)] for f_T in their experiments on frog sartorius muscles, and this value was used to estimate the basic fiber parameters G_T and R_{sm}. Also data of Adrian and Freygang (1962) were used to obtain a relationship between changes in membrane potential and "instantaneous" (post-capacity transient) conductance.

In practice, a particular fiber was selected from the muscle and the three internal electrodes positioned appropriately in it. Initially, 100-msec constant-voltage pulses of about 15 mV and constant-current pulses of about 3 $\mu A \cdot cm^{-2}$ were used and the electrode potentials recorded on film from the oscilloscope so that from V_2, I_0 and $(V_2 - V_1)$ the fiber radius a and the effective membrane resistance R_m could be calculated and so enable calculation of R_{sm} and $\bar{G}_W$. In fibers 1 through 9 only short hyperpolarizing pulses were used whereas in fibers 11 through 19 both hyperpolarizing and depolarizing pulses were used so that in the latter experiments the resistance for currents in both directions was known. After the initial short pulses, the output was switched to a Biomac pulse averaging computer (Biomac, Data Laboratories Ltd., London, England) and long pulses of either 2- or 4-sec duration were used. The final pulses recorded on film for both voltage-clamp (about 15 mV as in the short pulses) and current-clamp hyperpolarizing pulses (again about 3 $\mu A \cdot cm^{-2}$) were the averages of eight pulses in each case. Tracings were made onto graph paper from an enlargement of the film negatives. The membrane throughout the rest of each experiment was clamped at the initial resting membrane potential and the unclamped resting potential checked again at the end of the experiment. The electronics was arranged so that the muscle fiber could simply be switched from the current-clamp mode to the voltage-clamp mode and vice-versa.

The experiments were all carried out with a solution temperature of 20 ± 0.5 °C. The solution used was a 2.5 mM K_2SO_4 solution (*see* solution B of Adrian *et al.*, 1970*a*) with the following ionic composition in $mM \cdot liter^{-1}$: K^+ 2.5; Na^+ 190; Ca^{2+} 9; HPO_4^{2-} 1.08; $H_2PO_4^-$ 0.43; SO_4^{2-} 104, and the addition of Tetrodotoxin (TTX) at a concentration of 10^{-6} g·ml^{-1} to block action potentials.

The fiber parameters and the analytical expressions resulting from the theoretical predictions were evaluated using a PDP-8/I computer or, in some cases, a Hewlett-Packard 9100 B programmable calculator, whereas the numerical solutions were computed using Fortran IV on an IBM 360/50 (University of N.S.W.) and an Atlas-Titan Computer (University of Cambridge).

Principles of Theory

Whenever a current crosses a membrane separating two solutions it will almost invariably cause changes in the ion concentrations adjacent to the membrane due to transport number effects because under almost no circumstances are the adjacent layers of solution perfectly stirred. Even with simple planar membranes there may be effective unstirred layers of the order of at least 10 to 1,000 μm.

The transport number effect itself (*see* Barry & Hope 1969*a*, *b*; *cf. also* Dewhurst, 1960) is illustrated in Fig. 1. If a membrane, for example, separates solutions of KCl and is itself predominantly permeable to K^+, then as a current is passed across the membrane there will be an increase in concentration relative to the bulk and initial concentrations on the right side and a decrease on the left side adjacent to the membrane as indicated in the figure. The rate of production of KCl, Φ_{KCl}, for a current of i amps·cm^{-2} will be given by:

$$\Phi_{KCl}=\frac{(t_K^m-t_K^s)}{F}i=-\frac{(t_{Cl}^m-t_{Cl}^s)}{F}i \tag{12}$$

in moles of KCl·cm^{-2}·sec^{-1} and an equal loss of KCl on the left side where t_K and t_{Cl} refer to the transport numbers of K^+ and Cl^- and the superscripts m

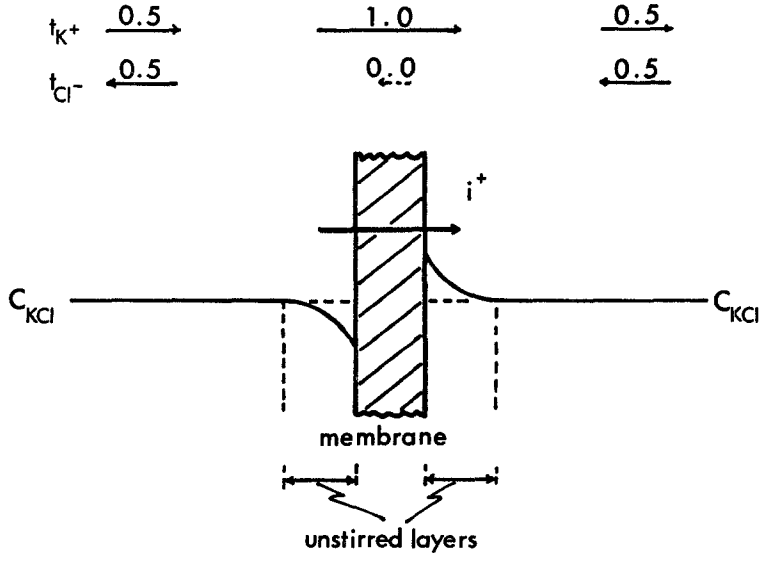

Fig. 1. A schematic diagram illustrating the transport number effect for a simple cation permeable membrane separating solutions of KCl. The transport numbers for K^+ and Cl^-, t_{K^+} and t_{Cl^-}, respectively, are shown and magnitudes and direction of their contribution to the total current i^+ are represented by the lengths of the solid arrows. Enhancement and depletion of KCl in the unstirred regions adjacent to the membrane are indicated

and s refer to the values in the membrane and solution, respectively. It should be noted that Eq. (12) automatically preserves electroneutrality. The loss of KCl will of course be balanced primarily by diffusion of KCl into the bulk solutions (*see* Barry & Hope, 1969*a*).

Now the TTS of a muscle fiber is a completely unstirred region and because of its large surface area represents a considerable fraction of the fiber conductance. In fact, when a fiber is placed in a SO_4^{2-} Ringer's solution without Cl^- ions the tubular K^+ conductance corresponds to about 66% of the total fiber conductance (Eisenberg & Gage, 1969). It would therefore be expected that there should be considerable changes in the ionic concentrations of the TTS due to transport number effects during the passage of current into a fiber. As we have already mentioned, experiments have shown that the tubules are open as far as the diffusion of molecules or ions are concerned (Huxley, 1964; Page, 1964; Endo, 1966). Following Adrian *et al.* (1969) we will consider the following model as representing a fairly good approximation to a muscle fiber.

Provided the tubules form a regular mesh network where the diameter of the tubules is taken to be small compared to the mesh and the mesh itself small compared to the diameter of the fiber itself, Adrian *et al.* (1969) have suggested that one should be able to approximate such a mesh of tubules by an equivalent homogeneous TTS disc[1], whose parameters can be related to the actual parameters of the TTS and whose width we will define as d cm. The effective conductance $\bar{G}'_W$ per cm^2 of equivalent disc for 1 cm^2 of fiber surface area is shown in Appendix A to be given by:

$$\bar{G}'_W = \frac{\frac{\rho}{\xi} G_W}{4\pi a} = \frac{\bar{G}_W}{4\pi a} \tag{13}$$

where $\bar{G}_W$, the conductance of the TTS per unit volume of fiber, is defined as

$$\bar{G}_W = \frac{\rho}{\xi} G_W \tag{14}$$

where G_W is the actual conductance of the walls of the TTS in mho·cm^{-2}, ρ is the volume fraction of the TTS and ξ is the volume-to-surface ratio of the TTS. Since the actual volume of the TTS should equal the volume of

1 As suggested in Appendix A this can be extended to n equivalent discs. The factor n, however, does not appear in any of the final equations and nor does d. Thus, there is no loss in generality in only considering one disc and it is more convenient for diagrams and discussion to do so.

this equivalent disc, the thickness d is related to ρ by

$$d=\rho/2\pi a. \tag{15}$$

Similarly, the effective diffusion coefficient D'_K and the lumen conductivity G'_L for the equivalent disc will be related to the actual parameters of the TTS by:

$$D'_K=\sigma D_K \tag{16}$$

$$G'_L=\sigma G_L \tag{17}$$

with $\sigma\approx 0.5$ for a number of different types of mesh (Adrian *et al.*, 1969).

Two further reasonable assumptions will be made: concentration changes on the sarcoplasm side of the tubular wall and at either side of the surface membrane will be neglected; the conductivity of the sarcoplasm is high and hence over the small region clamped experimentally it will be considered as equipotential.

Consider the volume elements of the TTS illustrated in Fig. 2 and its schematic electrical circuit in Fig. 3. It will be assumed that the tubular wall is permeable only to K^+ ions. This should be a good approximation for inward current for a muscle fiber in a K_2SO_4 Ringer's solution. It may not be so good an approximation for outward current in the high resistance direction as there may then be some other ion contributing to the current. The experimentally used values of K^+ conductance and the estimated magnitudes of the transport number effects may then be somewhat overestimated for outward currents, but the "on part" of the hyperpolarizing currents should not be affected. If then a voltage or current pulse is applied as shown in the two figures, since the concentration of K^+ in the tubular lumen is low compared to both Na^+ and SO_4^{2-} ions, the K^+ transport number difference between the membrane t_K^m and the luminal solution t_K^s becomes:

$$t_K^m-t_K^s\approx 1.$$

Hence, the loss in moles of K^+ in the volume element (Fig. 2) due to the transport number effect is from Eq. (12)

$$\frac{2\cdot 2\pi r\,dr(t_K^m-t_K^s)I_K(r)}{F}\approx\frac{4\pi r\,dr\,I_K(r)}{F}$$

where $I_K(r)$ is the K^+ current density across the equivalent TTS disc at radial distance r. The current will be defined as positive when it is in the

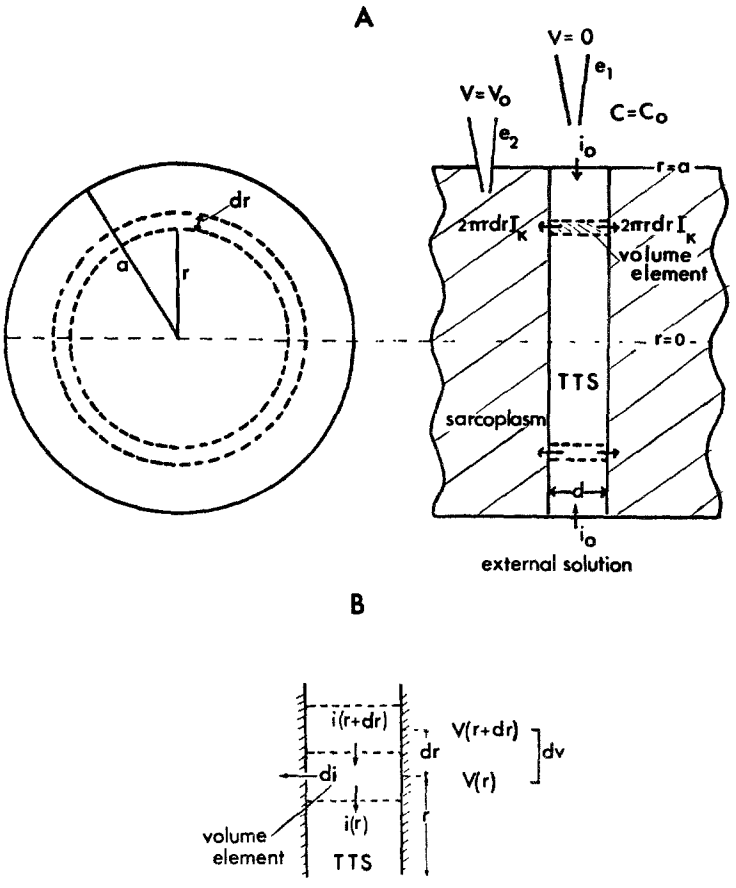

Fig. 2. (*A*) A cross-section and longitudinal section of the equivalent disc (thickness d) representing the transverse tubular system (TTS) in a muscle fiber of radius a. The volume ring element of thickness dr at a radial distance r is shown together with the electrical set-up. The latter is shown schematically as the two electrodes e_1 and e_2 in the external solution (potential, V, $=0$) and the sarcoplasm (potential, V, $=V_0$), respectively. The total current entering the TTS, i_0, and the K^+ current crossing the two walls of the volume element are shown; I_K refers to the K^+ current density passing across the walls of the disc; C_0 the K^+ concentration in the external solution. (*B*) An enlargement of part of the volume element, shown in the longitudinal section in Fig. 2*A*, shows the reduction of radial current $di(r)$, and changes in the lumen potential $dV(r)$ across the ring element, caused by the K^+ current across its walls

hyperpolarizing inward (TTS-to-sarcoplasm) direction, which is the opposite convention to that used by Adrian *et al.* (1969). This loss balanced by the increase in the number of moles of K^+ in the volume element due to diffusion is given by:

$$\sigma D_K d \frac{\partial}{\partial r}\left(2\pi r \frac{\partial C}{\partial r}\right) dr$$

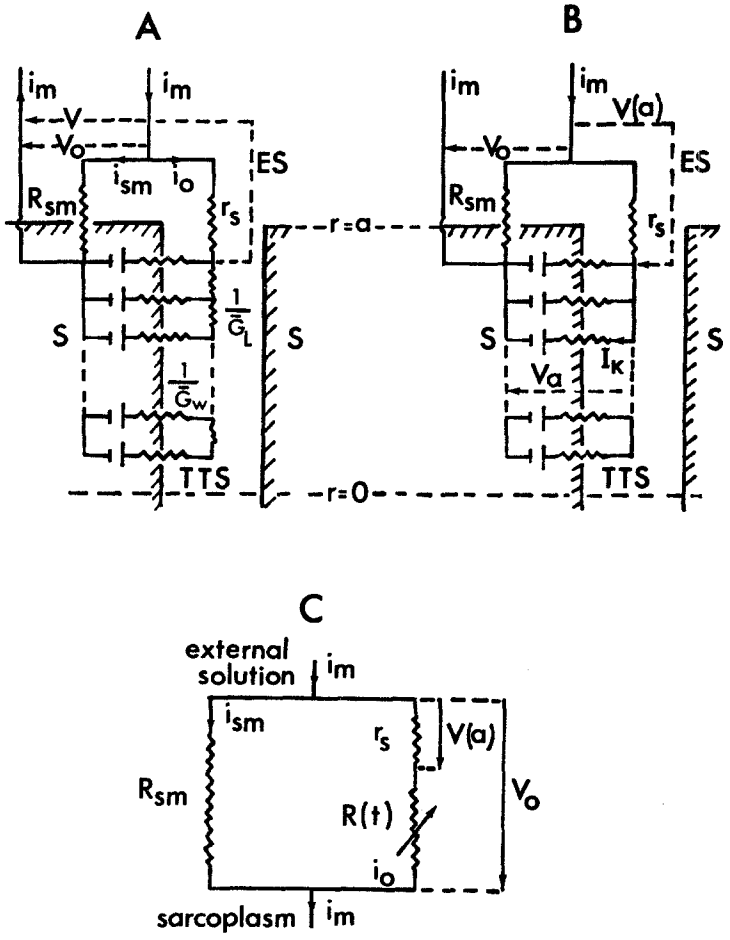

Fig. 3. (*A*) A full schematic electrical circuit diagram of the equivalent TTS disc shown in Fig. 2*A* and used for the numerical analysis and the steady-state mathematical analysis. The symbols are explained in the text and it is assumed that the external solution (*ES*) and the sarcoplasm (*S*) have a high enough conductivity as to be considered equipotential. (*B*) The circuit diagram is the same as that shown in Fig. 3*A* except that now the lumen of the TTS is also considered as equipotential. This circuit was the one assumed for the time-dependent mathematical analysis. (*C*) The overall lumped electrical circuit of Figs. 3*A* and 3*B*

where C is the concentration of K^+ within the TTS at radial distance r. Hence the increase in the number of moles of K^+ in this volume element will be

$$2\pi r dr \cdot d\frac{\partial C}{\partial t}.$$

Hence, the actual rate of increase of concentration will be given by the full equation of continuity which becomes with a little simplification:

$$\rho \frac{\partial C}{\partial t} = \sigma \rho D_K \frac{1}{r} \frac{\partial}{\partial r}\left(r \frac{\partial C}{\partial r}\right) - \frac{4\pi a I_K}{F} \tag{18}$$

since $d = \rho/2\pi a$ from Eq. (15) and where C is finite when $r=0$, and $C=C_0$ (the initial and bulk K^+ concentration) for all r at $t=0$.

Now as far as the current-voltage equations are concerned from current continuity considerations (*see* Figs. 2 and 3)

$$di(r,t) = 2I_K 2\pi r dr = \frac{\partial i(r,t)}{\partial r} dr.$$

Hence,

$$I_K = \frac{1}{4\pi r} \frac{\partial i(r,t)}{\partial r}. \tag{19}$$

At the same time the resistive drop from one element to the next dR over a distance dr (*see* Figs. 2 and 3) will cause a voltage drop dV given by

$$dV = idR = \frac{idr}{2\pi r \sigma G_L d} = \frac{aidr}{r\sigma\rho G_L} = \frac{aidr}{r\bar{G}_L}$$

where $\bar{G}_L$ is defined as

$$\bar{G}_L = \sigma \rho G_L. \tag{20}$$

Hence,

$$\frac{\partial V(r,t)}{\partial r} = \frac{a}{r} \frac{i}{\bar{G}_L}. \tag{21}$$

By multiplying both sides of Eq. (21) by r, taking its derivative and then substituting from Eq. (19) the cable equation for the radial change in voltage in the TTS becomes:

$$\frac{1}{r} \frac{\partial}{\partial r}\left(r \frac{\partial V}{\partial r}\right) = \frac{4\pi a}{\bar{G}_L} I_K \tag{22}$$

where V is finite when $r=0$, and where both V and I_K are functions of r and t. Now if, when there is no externally applied voltage or current, K^+ is in equilibrium so that I_K is zero, then

$$I_K \approx 0 \approx -G'_W\left(V_{OA} - \frac{RT}{F} \ln\left(\frac{C_o}{C_{OA}}\right)\right)$$

where V_{OA} is the absolute resting p.d. between the sarcoplasm and the external solution, C_{OA} is the absolute value of the K^+ concentration within the sarcoplasm and C_o is the K^+ concentration in the tubular system assumed to be the same as in the external solution before the onset of a current or voltage pulse.

If we henceforth define all voltages as the change in voltage from their resting values then when a current or voltage pulse is applied to a fiber this K^+ current I_K across the tubular wall will be given, substituting for G'_W from Eq. (13), by

$$I_K = -\frac{\bar{G}_W}{4\pi a}\left(V_0 - V(r,t) - \frac{RT}{F}\ln\left(\frac{C(r,t)}{C_o}\right)\right) \tag{23}$$

where $V(r, t)$ and V_0, which will be time-dependent during constant-current pulses, refer to changes in potential in the TTS and sarcoplasm, respectively, with respect to the external solution, and where $\bar{G}_W$ may or may not be a function of the driving force

$$V_0 - V(r,t) - \frac{RT}{F}\ln\left(C(r,t)/C_o\right) \equiv \Delta V - E_K$$

where E_K is the K^+ equilibrium potential and ΔV the p.d. across the tubular wall.

Boundary Conditions

It seems likely that the TTS has a finite access resistance (Peachey & Adrian, 1973). Such an access resistance might be expected purely from geometrical considerations of the number of tubules actually opening out at the fiber surface. Such a possibility or any other type of effective resistance due to geometry at the fiber surface may be approximated by assuming that there is a small length of tubules δ near the surface where the tubules are elongated and/or constricted by a geometry or tortuosity factor θ. Now the resistance of this access element r_s per unit surface area of fiber will be given by:

$$r_s = \frac{\delta}{2\pi a \sigma G_L \theta d} = \frac{\delta}{\theta \sigma \rho G_L} = \frac{\delta}{\theta \bar{G}_L} \tag{24}$$

[remembering Eqs. (15) and (20)].

Thus, from Eq. (21) at $r = a$ from current continuity considerations

$$i = \frac{-V(a)}{r_s} = \frac{\partial V}{\partial r}\Big)_{r=a} \bar{G}_L$$

so that

$$\left.\frac{\partial V}{\partial r}\right)_{r=a} = \frac{-V(a)}{r_s \bar{G}_L} \tag{25}$$

where $V(a)$ refers to the p.d. just at the internal end of the access resistance ($r=a$), as indicated in Figs. 3*A* and *C*, with respect to the potential in the external solution.

Assuming that the same geometry factors apply for K^+ diffusion at the fiber surface then the radial flux of K^+ will be given by

$$\frac{\sigma D_K \theta (C_o - C(a)) 2\pi a d}{\delta} = 2\pi a d \sigma D_K \left.\frac{\partial C}{\partial r}\right)_{r=a}$$

so that

$$\left.\frac{\partial C}{\partial r}\right)_{r=a} = \frac{C_o - C(a)}{h \bar{D}_K} \tag{26}$$

where by definition

$$h \equiv \frac{\delta}{\bar{D}_K \theta} \tag{27}$$

and

$$\bar{D}_K \equiv \sigma \rho D_K, \tag{28}$$

$\bar{D}_K$ now being the effective radial component of diffusion for K^+ referred to 1 cm^2 of surface membrane.

From Eqs. (24) and (28) h may be expressed in terms of the electrical access resistance r_s by

$$h = \frac{r_s \bar{G}_L}{\bar{D}_K}. \tag{29}$$

If there was no access resistance[2] then $r_s = 0$ and the boundary conditions instead of being Eqs. (25) and (26) together with Eq. (29) would simply become (*see* Fig. 3*C*)

$$V(a) = 0 \tag{30}$$

and

$$C(a) = C_o. \tag{31}$$

Effects of Longitudinal Branching

Peachy and Schild (1968) and Eisenberg and Eisenberg (1968) have shown that the tubular system has in addition to the transverse tubules a significant component of longi-

2 The effect on the predicted conductance changes of reducing the access resistance to zero while leaving the total radial resistance unaltered is discussed on pp. 281–282 and shown in Table 5.

tudinal tubules. Peachey and Schild estimated that the component of longitudinal tubules represented about 30% of the volume of the transverse tubules alone, and although there are some uncertainties about the accuracy of such estimates (*see* Eisenberg & Eisenberg, 1968), such a value will be used in this paper. Such longitudinal branching would of course have no effect on the radial components of diffusion or electrical conductance. Thus it would not affect Eqs. (22) or (23) nor would it affect the boundary conditions. However, it would tend to dilute the K^+ concentration so that Eq. (18) should really become

$$\rho' \frac{\partial C}{\partial t} = \sigma \rho D_K \frac{1}{r} \frac{\partial}{\partial r} \left(r \frac{\partial C}{\partial r} \right) - \frac{4\pi a I_K}{F} \tag{32}$$

where ρ is the volume fraction of the TTS and ρ' is the volume fraction of the whole tubular system including longitudinal branching. This tacitly assumes perfect mixing in the longitudinal direction, which is a reasonable assumption since sarcomere length is very much less than fiber radius. Since in every term of the basic equations, with the exception of the left-hand term of the above equation, σ and ρ appear together as $\sigma\rho$ and σ never appears on its own, the simplest way of including the effects of longitudinal branching is to leave the equations as they were without taking it into account but when the parameters are being substituted into the final solutions to make the following modifications. For example, if longitudinal branching is considered to increase the total tubular volume to 4/3 times the TTS volume, then ρ should be increased to 4/3 its TTS value and σ decreased to 3/4 of its original value so that in fact $\sigma\rho$ remains unchanged from its original TTS values. For this reason the following treatment will not explicitly include the effects of longitudinal branching.

Analytical Solutions

Steady-State Solution

In the steady state after the onset of an electrical pulse, when the membrane voltage and current are no longer changing then

$$\frac{\partial C}{\partial t} = 0. \tag{33}$$

It then immediately follows from Eqs. (18) and (22) that

$$\frac{d}{dr}\left(r \frac{dV}{dr} \right) = \frac{F\bar{D}_K}{\bar{G}_L} \frac{d}{dr}\left(r \frac{dC}{dr} \right)$$

which on integration, together with the boundary conditions at $r=a$ [Eqs. (25), (26) and (29)] and the condition that both C and V are finite at the center of the fiber ($r=0$) becomes:

$$V(r) = \frac{F\bar{D}_K}{\bar{G}_L} (C(r) - C_o). \tag{34}$$

This very simple relationship, which holds also for the boundary conditions of Eqs. (30) and (31) (i.e., $r_s=0$), together with the assumption that the TTS wall conductance G_W is independent of driving force $\Delta V-E_K$ [*see* Eq. (23)] and an approximation of the logarithm in Eq. (23), enables Eqs. (18), (21) and (23) to be solved. The logarithm approximation takes the first two terms of the series expansion for $\ln(1+x)$ viz:

$$\ln\left(\frac{C(t)}{C_o}\right)=\ln\left(1+\left(\frac{C(t)-C_o}{C_o}\right)\right)\approx-\left(1-\frac{C(t)}{C_o}\right). \tag{35}$$

It is a good approximation provided that

$$\left|\frac{C(t)-C_o}{C_o}\right|\ll 1.$$

In practice this will later be shown to predict membrane resistances accurate to within approximately 5% for a voltage pulse of -20 mV.

The solution of these equations will be published later. However, it can readily be shown that the total membrane current into a fiber i_m is related to the applied p.d., V_0, between the sarcoplasm and the bathing solution by:

$$i_m=-V_0\left[\frac{1}{R_{sm}}+\frac{\bar{G}_W\lambda_T I_1(a/\lambda_T)}{\left\{I_0(a/\lambda_T)+\frac{r_s\bar{G}_L}{\lambda_T}I_1(a/\lambda_T)\right\}}\right] \tag{36}$$

where λ_T, a length constant describing the radial drop in the potential profile within the TTS, is given by

$$\lambda_T^2=\frac{\bar{G}_L}{\bar{G}_W\left[1+\frac{RTG_L}{F^2D_K C_o}\right]}. \tag{37}$$

The term "$-V_0/R_{sm}$" in Eq. (36) represents the inward current going through the surface membrane of the fiber for such a hyperpolarizing pulse.

Provided that $RTG_L/(F^2D_K C_o)\gg 1$, Eqs. (36) and (37) become identical with the time-dependent solutions which needed the assumption that within the TTS there was infinite conductivity. That is: Eq. (37) becomes equivalent to Eq. (44) and Eq. (36) becomes equivalent to either Eq. (43) or Eq. (61). In addition, if $r_s=0$ and the surface membrane current is not included then Eqs. (36) and (37) reduce to an unpublished equation derived by Dr. Knox Chandler (*personal communication*) for the same problem but using a slightly different approach.

The instantaneous (post-capacity transient) current-voltage relationship may be deduced by considering the effect of hypothetical perfect stirring within the TTS. The introduction of such perfect stirring in the TTS is *formally* equivalent to increasing the diffusion coefficient to infinity while keeping all the other parameters unchanged. (Of course experimentally D_K and G_L are directly related, but such a relationship has not been used in the analysis.) Then Eqs. (36) and (37) become simply

$$i_m = -\frac{V_0}{R_{sm}} - \frac{\bar{G}_L V_0 I_1(a/\lambda_T)}{\lambda_T I_0(a/\lambda_T) + r_s \bar{G}_L I_1(a/\lambda_T)} \tag{38}$$

with

$$\lambda_T = (\bar{G}_L/\bar{G}_W)^{\frac{1}{2}}. \tag{39}$$

If $r_s = 0$, the current direction is redefined (positive if outward) and the surface membrane current is not included then Eqs. (38) and (39) reduce simply to Eq. (12) of Adrian *et al.* (1969).

Time-Dependent Solutions

To solve the time-dependent equations [i.e. Eqs. (18), (22) and (23)] for K^+ depletion in addition to the assumption of a constant conductance and the logarithmic approximation [Eq. (35)] made for the steady-state analysis, it is necessary to assume that the resistivity of the lumen of the tubules is small enough that it can be neglected. Actually, a comparison of the initial and infinite time values of the TTS resistance obtained from time-dependent solutions making this assumption with those obtained using the direct steady-state equation [Eqs. (36) and (37)] indicated that this assumption only caused an error of approximately 1% for the initial TTS resistance and approximately 0.5% for the final steady-state TTS resistance. With this additional assumption then, the circuit diagram of the fiber thus simplifies from that shown in Fig. 3*A* to that in Fig. 3*B*.

I. Constant-Voltage Case. We now have Eqs. (18), (22), (23), (25), (26) and (29) and can replace Eq. (22) with

$$i_0 = 2\int_0^a 2\pi r I_K \, dr \tag{40}$$

where i_0 is the current going through the TTS.

The solution of these equations will be published later and can be shown to be

$$i_m(t) = i_{sm} + i_0 = -G_m(t) V_0 \tag{41}$$

where

$$G_m(t)=G_m(\infty)-G_t(\alpha)\,e^{-(\phi-\alpha^2)t}-\sum_{m=1}^{\infty}G_t(i\alpha_m)\,e^{-(\phi+\alpha_m^2)t} \tag{42}$$

$$G_m(\infty)=G_{sm}+\frac{\bar{G}_W\lambda_T I_1(a/\lambda_T)}{\left[\left\{I_0(a/\lambda_T)+\dfrac{r_s\bar{G}_L}{\lambda_T}I_1(a/\lambda_T)\right\}+r_s\bar{G}_W\lambda_T I_1(a/\lambda_T)\right]} \tag{43}$$

where $G_{sm}=1/R_{sm}$, and *now* [*Cp.* Eq. (37)]:

$$\lambda_T^2=\bar{D}_K F^2 C_o/(\bar{G}_W RT) \tag{44}$$

where λ_T again represents a type of length constant describing the drop in the concentration profile of K^+ (but not the potential profile in the TTS which is now for convenience assumed to be equipotential) towards the center of the TTS, and

$$G_t(\alpha)=\frac{4\phi\bar{G}_W\alpha^2}{(\phi-\alpha^2)M(\alpha,\omega)} \tag{45}$$

with

$$\begin{aligned}M(\alpha,\omega)=&\frac{2a'\alpha^2}{a}(1-\alpha^2v'^2)[\alpha^2-a\omega(\phi-\alpha^2)]-4\phi\omega(a'v'\alpha^2+2)\\&+a\omega^2\left[\frac{a'^2}{2}(\phi-\alpha^2)^2(1-\alpha^2v'^2)-2\phi\{(a'v'\alpha^2+2)-a'v'\phi\}\right]\end{aligned} \tag{46}$$

and where $G_t(i\alpha_m)$ and $M(i\alpha_m)$ are obtained by replacing α by $i\alpha_m$ in Eqs. (45) and (46), i being the $\sqrt{-1}$. The values of α and α_m are the solutions of the two Bessel function equations:

$$A(\alpha)I_0(a'\alpha)-[2\omega\phi-\alpha v'A(\alpha)]I_1(a'\alpha)=0 \tag{47}$$

with

$$A(\alpha)=\omega a'\alpha(\phi-\alpha^2)-2\alpha^3a'/a \quad \text{for } 0<\alpha^2<\phi \tag{48}$$

and

$$A(i\alpha_m)J_0(a'\alpha_m)-[2\omega\phi+\alpha_m v'A(i\alpha_m)]J_1(a'\alpha_m)=0 \tag{49}$$

with

$$A(i\alpha_m)=\omega a'\alpha_m(\phi+\alpha_m^2)+2\alpha_m^3a'/a \quad \text{for } 0<\alpha_m^2 \tag{50}$$

where $J_0(a'\alpha_m)$ and $J_1(a'\alpha_m)$ are the ordinary Bessel functions of order "0" and "1" (*cf.* Abramowitz & Stegun, 1965) and the other variables are defined as follows:

$$\omega=r_s\bar{G}_W \tag{51}$$

$$a'=a/(\bar{D}_K/\rho)^{\frac{1}{2}} \tag{52}$$

$$v' = r_s \bar{G}_L / (\bar{D}_K/\rho)^{\frac{1}{2}} \tag{53}$$

$$\phi = \bar{G}_W RT/\rho F^2 C_o. \tag{54}$$

From Eqs. (23) and (40) the "instantaneous" total membrane conductance is given by

$$G_m(0) = G_{sm} + \frac{\bar{G}_W a}{(2 + r_s \bar{G}_W a)}. \tag{55}$$

A good check of Eqs. (41) through (54) is that they should reduce to Eq. (55) as $t \to 0$. The comparison was made numerically and the agreement for resulting "instantaneous" conductances was found to be better than one part in 10^8 [the order expected from the rounding-off errors resulting from the 69 terms used for the series summation of Eq. (42)].

II. Constant-Current Case. Since V_0 is now no longer constant, both i_{sm} and i_0 are now time-dependent, varying in such a way as to keep the total membrane current i_m constant; i.e.

$$i_m = i_{sm}(t) + i_0(t) \tag{56}$$

where

$$i_{sm}(t) = -V_0(t)/R_{sm}. \tag{57}$$

Now Fig. 3*C* shows clearly that

$$V(a, t) = -r_s i_0(t). \tag{58}$$

The solution of Eqs. (18), (23), (25), (26), (29) and (40) together with Eqs. (56) through (58) will be published later and can be shown to be

$$V_0(t) = -R_m(t)\, i_m \tag{59}$$

where $R_m(t)$ is given by

$$R_m(t) = R_m(\infty) + R(\alpha)\, e^{-(\phi - \alpha^2)t} + \sum_{m=1}^{\infty} R(i\alpha_m)\, e^{-(\phi + \alpha_m^2)t} \tag{60}$$

where

$$R_m(\infty) = \frac{R_{sm}\left[I_0(a/\lambda_T) + \left(\frac{r_s \bar{G}_L}{\lambda_T} + r_s \bar{G}_W \lambda_T\right) I_1(a/\lambda_T)\right]}{\left[\left\{I_0(a/\lambda_T) + \left(\frac{r_s \bar{G}_L}{\lambda_T} + r_s \bar{G}_W \lambda_T\right) I_1(a/\lambda_T)\right\} + \bar{G}_W R_{sm} \lambda_T I_1(a/\lambda_T)\right]} \tag{61}$$

with

$$R(\alpha) = \frac{4\phi \bar{G}_W R_{sm}^2 \alpha^2}{(\phi - \alpha^2) M(\alpha, \omega)} \tag{62}$$

and

$$M(\alpha,\omega')=\left[\frac{2a'^2\alpha^2}{a}(1-\alpha^2v'^2)(\alpha^2-a\omega'(\phi-\alpha^2))-4\omega'\phi(a'v'\alpha^2+2)\right.$$
$$\left.+a\omega'^2\left\{\frac{a'^2(\phi-\alpha^2)^2(1-\alpha^2v'^2)}{2}-2\phi((a'v'\alpha^2+2)-a'v'\phi)\right\}\right] \tag{63}$$

and where again $R(i\alpha_m)$ and $M(i\alpha_m, \omega')$ are obtained by replacing α by $i\alpha_m$ in Eqs. (62) and (63), i again being $\sqrt{-1}$, and where now ω' is defined as

$$\omega'=\bar{G}_W(R_{sm}+r_s) \tag{64}$$

the α and the α_m being given by the solutions of

$$A(\alpha)I_0(a'\alpha)-[2\omega'\phi-\alpha v'A(\alpha)]\ I_1(a'\alpha)=0 \tag{65}$$

with

$$A(\alpha)=\omega'a'\alpha(\phi-\alpha^2)-2a'\alpha^3/a \quad \text{for } 0<\alpha^2<\phi \tag{66}$$

and

$$A(i\alpha_m)J_0(a'\alpha_m)-[2\omega'\phi+\alpha_m v'A(i\alpha_m)]\ J_1(a'\alpha_m)=0 \tag{67}$$

with

$$A(i\alpha_m)=\omega'a'\alpha_m(\phi+\alpha_m^2)+2a'\alpha_m^3/a \quad \text{for } 0<\alpha_m^2 \tag{68}$$

where all the other terms are the same as before. The obvious similarity between the constant-current and constant-voltage equations arises from the fact that letting the surface membrane resistance R_{sm} become very small and close to but not equal to 0 in the constant-current case tends to be effectively the same as voltage clamping the fiber and in fact under this condition Eqs. (56) through (68) do transform to Eqs. (41) to (50) (Appendix B). Again Eqs. (56) through (68) should reduce to Eq. (55) as $t \to 0$. The comparison was again made numerically and agreement found to better than five parts in 10^9 using 44 terms of the series in Eq. (60).

Predictions of Analytical Solutions

The average parameters of a number of muscle fibers measured during these experiments and the TTS parameters discussed and justified in a later section of the paper had the following values:

$G_L=10^{-2}$ mho · cm^{-1}

$\rho=0.0030$ (with an additional 0.0010 for the volume of the longitudinal tubules)

$$\sigma = 0.50$$

$$a = 51\ \mu\text{m}$$

$$r_s = 100\ \Omega\ \text{cm}^2$$

$$R_{sm} = 19.41\ \text{K}\Omega\ \text{cm}^2$$

$$C_K = 2.5\ \text{mM} \cdot \text{liter}^{-1}$$

$$\bar{G}_W = 0.040\ \text{mho} \cdot \text{cm}^{-3}.$$

These parameters will be referred to as "model fiber parameters" and were very similar to the average parameters of Table 2 where $a = 52\ \mu\text{m}$, $R_{sm} = 20\ \text{K}\Omega\ \text{cm}^2$ and $\bar{G}_W = 0.038\ \text{mho} \cdot \text{cm}^{-3}$.

In practice the effect of the longitudinal tubule volume was taken into account as indicated in the previous section "Effects of Longitudinal Branching" by increasing ρ to 0.0040 and decreasing σ to 0.375 so that $\sigma\rho$ was still 1.5×10^{-3}.

Equations (47) through (50) and (65) through (68) were solved numerically using a simple iterative procedure and together with the other equations were evaluated using a small PDP-8 computer or where greater accuracy was required a Hewlett-Packard 9100 B programmable calculator. In each case the series equations at $t = 0$ were compared with those obtained directly [Eq. (55)] and were found to agree to within one part in 10^6 on the PDP-8 or one part in 10^8 on the Hewlett-Packard machine indicating that no terms in the series had been miscalculated or roots omitted. This was particularly important since as far as the PDP-8 was concerned its six-figure accuracy was in certain cases not adequate to find an existing α root, and there do exist sets of parameters for which there is no α root. The time constants could be obtained in one of two ways. The principal time constant τ, the time constant of the first time-dependent term of Eqs. (42) and (60) was obtained from

$$\tau = 1/(\phi - \alpha^2) \tag{69}$$

if there was an α root, or

$$\tau = 1/(\phi + \alpha_1^2) \tag{70}$$

if there was no α root.

Alternatively, the time-dependent curve could be evaluated and a least-squares regression line could be fitted to $\ln[G(t) - G(\infty)]$ *vs.* t. This was in fact the method used to analyze the experimental records and as in the

Table 1. Approximate solutions using the mathematical analysis for K^+ depletion in the tubules of the model fiber [a]

Parameter	Notes	Value	Eqs. used
$R_m(t=0)$	[b]	6.59 KΩ cm^2	(38) & (39)
$R_m(t=\infty)$	[b]	10.14 KΩ cm^2	(36) & (37)
$\Delta G/G$	[b]	0.350	—
$R_m(t=0)$	[c]	6.56 KΩ cm^2	(55)
$R_m(t=\infty)$	[c]	10.13 KΩ cm^2	(43) or (61)
$\Delta G/G$	[c]	0.353	—
τ_{vc}	[c, d]	549 msec	(69) or (70), with (47)–(50)
τ_{vc}	[c, e]	543 msec	(42)–(50)
τ_{cc}	[c, d]	842 msec	(69) or (70), with (65)–(68)
τ_{cc}	[c, e]	835 msec	(59)–(68)

[a] This analysis used the logarithmic approximation and the assumption of a constant membrane conductance.
[b] $\bar{G}_L$ within the TTS is finite.
[c] $\bar{G}_L$ within the TTS is infinite.
[d] The time-constant was calculated from the principal term of the series.
[e] The time-constant was obtained from a regression curve over the range from 200 to 600 msec.

experimental analysis the 200- to 600-msec interval was used. Again the time constant was calculated from the regression line.

The results of such calculations are shown in Table 1 which indicates that, for a fiber in a 2.5 mM K_2SO_4 Ringer's solution, K^+ depletion should cause almost a halving of conductance with time constants of about 550 and 840 msec for voltage-clamp and current-clamp pulses, respectively. The magnitudes of the conductance change in both cases are not too far away from the values obtained experimentally (*cf.* Table 3) although the time constants, particularly the current-clamp ones, are somewhat longer than the experimentally observed ones. It may also be noted in Table 1 that the error in the predicted overall membrane resistance due to considering an infinite luminal conductivity in the bulk of the TTS is $<1\%$ (the normal value of $\bar{G}_L = 1.5 \times 10^{-5}$ was still used for relating the diffusion access resistance term to the electrical access resistance). Also, the principal time constant [the time constant of the first series term in Eqs. (42) and (60)] is almost identical with the time constant obtained by a regression analysis (*see* p. 272) from the 200- to 600-msec parts of the curves in both the voltage-clamp and current-clamp cases.

Fig. 4 shows an example of such an analytical solution using the TTS parameters already considered together with the parameters listed in Table 2

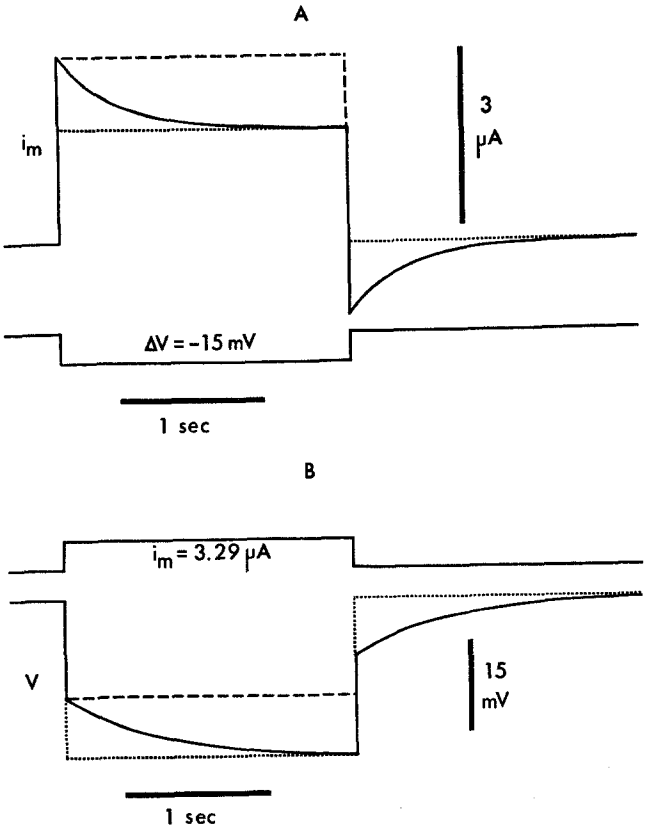

Fig. 4. (*A*) The membrane current i_m (considered per cm^2 of surface membrane) during a constant hyperpolarizing voltage pulse ($\Delta V = -15$ mV) of 2-sec duration calculated using the time-dependent mathematical analysis [Eqs. (42)–(50)] for the parameters measured for Fiber 5 (Table 2) and the other TTS parameters discussed in the text. The coarse dashed line indicates the current response during the voltage pulse if there is no K^+ depletion in the TTS. The response after the termination of the pulse was a computer simulation of the mathematical analysis using the same assumptions inherent in such an analysis. It indicates the symmetrical nature of the transient current response during and after the voltage pulse and in particular should be compared with Fig. 7 to show the inadequacy of the assumptions the mathematical analysis used in simulating the experimental current "tail". (*B*) The change in membrane potential V during a constant hyperpolarizing current pulse of 2-sec duration ($i_m = 3.29$ μAmp for 1 cm^2 of surface membrane) calculated using the time-dependent mathematical analysis [Eqs. (59)–(68)] for Fiber 5 with the same parameters as used for Fig. 4*A*. The coarse dashed line indicates the voltage response during the current pulse if there is no K^+ depletion in the TTS. Again the response after the termination of the pulse was a computer simulation of the mathematical analysis using the same assumptions inherent in such an analysis. In indicates the symmetrical nature of the transient voltage response during and after the current pulse and in particular should be compared with Fig. 8 to show the inadequacy of the assumptions of the mathematical analysis in simulating the experimental voltage "tail". During the onset of the current the voltage only reaches about 98.3% of its steady-state value and the marginal deviation from the resting voltage two seconds after the termination of the pulse (seen in the figure) is because of this

Table 2. Experimental parameters[a] for muscle fibers in a Na_2SO_4 Ringer's solution with a K^+ concentration of 2.5 mEquiv·liter^{-1}

Fiber no.	a (μm)	$\bar{G}_W$ (mho·cm^{-2})	R_{sm} (KΩ cm^2)	R_m (KΩ cm^2)	ΔV[b] (mV)	I_0[c] (μA·cm^{-2})	Membrane p. d.	
							Start of clamp	End of clamp
5	44.9±0.2	0.0603	14.68	4.99±0.06	15.6±0.1	3.29	88	70
7	30.8±0.04	0.0397	32.06	10.90±0.04	15.8±0.1	2.77	80	—
9	49.1±0.2	0.0503	16.06	5.46±0.13	15.6±0.1	3.36	80	65
14	67.4±0.6	0.0282	20.82	7.08±0.13	15.6±0.1	2.16	86	77
18	53.1±0.5	0.0405	18.41	6.26±0.22	15.1±0.1	3.20	87	83
19	66.5±1.5	0.0356	16.82	5.72±0.20	14.7±0.2	2.27	87	81
avg.	52 ±6	0.038	20.00	6.8 ±0.9	15.4±0.2	2.84±0.22	—	—
model[d]	51	0.040	19.41	6.6	—	—	—	—

[a] The errors given are the SEM. The radius a and membrane resistance R_m were calculated directly from the fast oscilloscope records taking R_i as 169 Ω cm and using Eqs. (1), (3)–(6) as discussed in the text. In every case including the averages, the tubular wall conductance $\bar{G}_W$, and surface membrane resistance R_{sm}, were calculated from the values of a and R_m taking f_T as 0.66, r_s as 100 Ω cm^2, $\bar{G}_L$ as 1.5×10^{-5} and using Eqs. (8), (10) and (11).

[b, c] V and I_0 represent the change in voltage during constant-voltage pulses and the membrane current during constant-current pulses.

[d] Model fiber parameters used for some of the theoretical calculations.

for one of the experimental fibers (Fiber 5). It shows clearly the symmetrical nature of the on and off responses of the membrane current which the analytical solution predicts, in contrast with the experimental curves in Fig. 7. Two assumptions however needed further investigation: First, the logarithmic approximation, and second, the assumption that the individual membrane conductance for K^+ ions was independent of the driving force $(V-E_K)$ on them. Whereas the latter is a good approximation for Rb^+ solutions it has been shown (Adrian & Freygang, 1962; Adrian, 1964) that in K^+ solutions there is a strong dependence of the K^+ conductance on the driving force $V-E_K$

Although Horowicz, Gage and Eisenberg (1968) have shown that the passive K^+ flux equation depends solely on the driving force $V-E_K$ on the K^+ ions, whether $V-E_K$ results from a variation in V or in E_K, it should be added that this does not preclude the possibility of the component of conductance which is independent of $V-E_K$ being dependent on the external K^+ concentration. For the sake of this analysis, in the absence of more data, it will be assumed as a first approximation that, over the estimated range for the average tubular K^+ concentration from 2.5 mM to 1.4 mM, this component is independent of the tubular K^+ concentration.

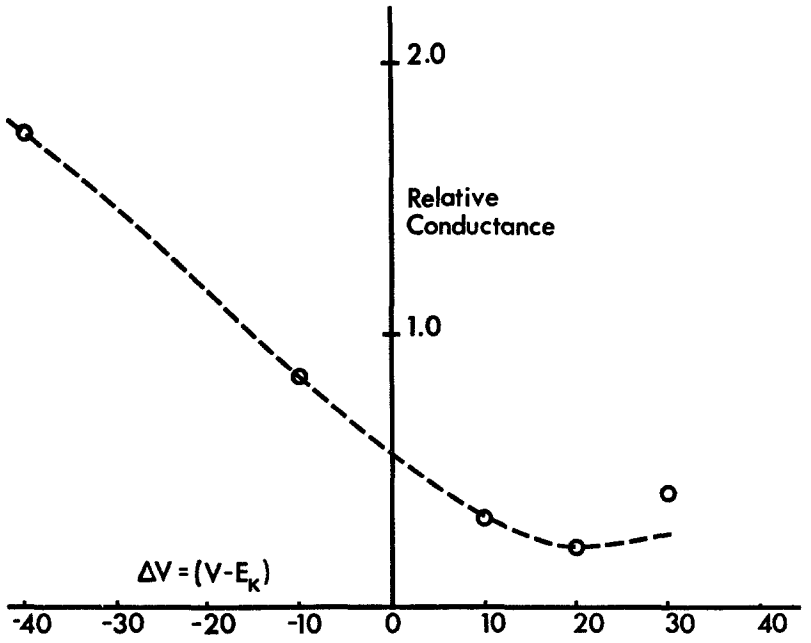

Fig. 5. The relative K^+ conductance of muscle fibers, measured as $(V_2-V_1)/V_1$ in three-electrode experiments, as a function of applied voltage ($\Delta V=V_1-E_K$). The points were obtained from the average values of Table 3 of Adrian and Freygang (1962) normalized to give the same value of conductance at $\Delta V=-40$ mV. The fibers were in a potassium-choline sulfate Ringer's solution. The dashed curve was fitted to the four points from -40 to $+20$ mV using Eq. (71) with $g_1=0.560$; $g_2=-25.6$; $g_3=323$; $g_4=4780$. This gave a relative conductance of 1.0 at -15 mV. This equation and these parameters were then used to compensate for changes in conductance with $(V-E_K)$ in the numerical analysis

The more important dependence of the K^+ conductance on the driving force $V-E_K$, is shown in Fig. 5 where the average values of the relative conductance of fibers from four different muscles (Table 3 of Adrian & Freygang, 1962) in a choline sulfate Ringer's solution (2.5 mM K, 0 mM Cl, 0 mM Na) have been plotted and may be fitted well by a cubic equation at least over the range between -40 mV to $+20$ mV, viz:

$$G(V-E_K)=g_1+g_2\cdot(V-E_K)+g_3\cdot(V-E_K)^2+g_4\cdot(V-E_K)^3. \qquad (71)$$

An inclusion of either or both of these corrections, however, would make the solution of the equations almost impossible if not impossible analytically. Yet, such an inclusion is necessary to attempt to explain the asymmetry between the time course of the current or voltage during the pulse with the recovery afterwards and indeed the asymmetry between hyper-

polarizing and depolarizing pulses. The equations, therefore, had to be solved using a numerical iterative procedure on a digital computer that could easily include such modifications.

Numerical Solutions

The numerical procedure involved dividing the fiber into m concentric rings (in practice $m=20$ or 40) and the use of numerical difference equations similar in principle to Eqs. (18) to (32) of the analytical analysis. The Fortran IV language (McCracken, 1965) was used. The time after the onset of a pulse was incremented in steps, Δt. At the beginning of each time step, after time t, the membrane current was computed and using a fourth-order Runge-Kutta routine (Ralston, 1965) the change in concentration and hence the new concentration in each of the m rings (numbered from the fiber surface inwards) was computed at the later time $t+\Delta t$. The actual Runge-Kutta equations used were, writing

$$\frac{dC_n}{dt}=f(t, C_n), \tag{72}$$

$$C_n(t+\Delta t)=C_n(t)+(K1_n+2\cdot K2_n+2\cdot K3_n+K4_n)/6 \tag{73}$$

where $f(t, C_n)$ is given by the difference between the increase in K^+ due to the transport number effect minus that lost due to radial diffusion [*cf.* Eqs. (18) and (23) of the mathematical analysis] and where

$$\begin{aligned} K1_n&=\Delta t\cdot f(t, C_n)\\ K2_n&=\Delta t\cdot f(t+\Delta t/2, C_n+K1_n/2)\\ K3_n&=\Delta t\cdot f(t+\Delta t/2, C_n+K2_n/2)\\ K4_n&=\Delta t\cdot f(t+\Delta t, C_n+K3_n). \end{aligned} \tag{74}$$

The equations used for the nth ring and evaluated in the current-finding subroutine were as follows:

$$VF_n\equiv V-E_K=V_0-V_n-\frac{RT}{F}\ln(C_n/C_o) \tag{75}$$

$$G_n=g_1+g_2\cdot VF_n+g_3\cdot VF_n^2+g_4\cdot VF_n^3 \tag{76}$$

where V_n and C_n represent the voltage and K^+ concentration, respectively, in the middle of the nth ring and where g_1, g_2, g_3 and g_4 are normalized so that when VF_n equals the voltage at which R_m was measured then the tubular wall conductivity per unit area of the equivalent disc, $G_n=\bar{G}_W$. Then

$$IT_n=-G_n\frac{(m-n+0.5)}{a}\Delta r^2 VF_n \tag{77}$$

$$IR_n=IR_{n-1}-IT_n \tag{78}$$

$$V_{n+1}=V_n-\frac{IR_n\cdot a\cdot\ln\{(m-n+0.5)/(m-n-0.5)\}}{G_L} \tag{79}$$

where IT_n represents the transverse current going through the center of the tubular wall of the nth ring and equivalent to dI in Fig. 2b; IR_n represents the radial current leaving the nth ring towards the center of the fiber; V_n is the p.d. at the center of the nth ring with respect to the external solution as opposed to being defined with respect to the sarcoplasm in the analytical treatment; and the ring thickness is given by

$$\Delta r = a/m. \tag{80}$$

In practice this current-finding subroutine made use of the condition that there should be zero radial current IR_m at the center of the fiber. Thus, if the correct value of the overall current was used the excess radial current IR_m, defined as ΔI, in the central ring should be zero. In fact, the excess current was found to be roughly proportional to the difference between the trial current used and the correct current. Thus, a particular value of the overall current I could be tried, a fraction β of the excess current ΔI then subtracted from I to get a new trial value of the overall current I', and the process repeated until $\Delta I/I$ was considered small enough, in practice $<10^{-6}$. As far as what fraction of ΔI should be used, in the voltage-clamp situation a rapid convergence of the routine was accomplished if $\beta=1$ so that

$$I' = I - \Delta I. \tag{81}$$

On the other hand, in the current-clamp situation this overcompensated and a reasonable convergence was obtained if $\beta=1/7$ so that

$$I' = I - \Delta I/7. \tag{82}$$

In practice also there was a maximum bound on the time increment for a given number of rings m or instability of the whole program would ensue. For example, if $m=20$, $\Delta t \lesssim 0.001$ sec and if $m=40$, then $\Delta t \lesssim 0.0005$ sec.

A comparison of the numerical analysis using the same approximations as assumed for the analytical analysis gave a good estimate of the accuracy of the program and it was found that for 20 rings error in the membrane conductance and resistance due to truncation errors was $\lesssim 0.1\%$ at the end of a 4-sec-long pulse. The program was run using double precision (16 decimal digits) on the IBM 360/50 or single precision (11 decimal digits) on the Atlas Titan computer. The full optimal program was still rather slow and using 20 rings, $\Delta t = 0.001$ sec took about 40 min for the onset and turn-off of a 4-sec-long voltage-clamp pulse and about 80 min for a 4-sec-long current-clamp pulse on the IBM 360/50 computer.

The predictions of this numerical analysis will be discussed in a later section in the paper.

Experimental Results

The experiments were carried out on a series of different fibers. Short (approximately 150 msec) pulses were used at the beginning of each experiment so that fiber radius a and the membrane resistance R_m could be calculated from the three-electrode response as discussed in the Methods section assuming the Nakajima and Hodgkin (1970) value of 169 Ω cm for the internal resistivity R_i. Then $\bar{G}_W$ and R_{sm} were calculated making use of the Eisenberg and Gage (1969) estimate for f_T of 0.66 for the fraction

of electrical conductance in the TTS. Then long constant-voltage and constant-current pulses were passed, of the same initial magnitude as the short pulses, between the sarcoplasm of the fibers and the external solution.

In fibers 5, 7 and 9 the long pulses were of approximately 2.0-sec duration whereas in fibers 14, 18 and 19 the pulses were of about 4.0-sec duration. In the former experiment, the sweep time of the Biomac averaging computer used for these long pulses was 5.12 sec whereas in the latter experiment it was 10.24 sec. There was also a delay at the end of every sweep of 10.24 sec and before each trigger pulse of 0.16 sec so that there was ample time for relaxation of concentration profiles after the termination of each pulse. Each of these long recorded traces was the average of eight pulses and for both constant-current and constant-voltage pulses the initial change in membrane potential in the hyperpolarizing direction was about 15 mV.

The following criteria were used to choose the six fibers shown in Tables 2 and 3: (1) Their membrane p.d. was at least −80 mV at the beginning of each experiment. (2) Both the averaged constant-current and constant-voltage traces had to have minimal membrane current ripple and no significant "kinks". (3) In addition, the ratio of the initial (post-capacitative) current trace (constant-current)/current trace (constant-voltage) from the short oscilloscope pulses at the beginning of the experiment were compared with the values obtained from the long Biomac pulses used for investigating the slow conductance changes. The voltage traces were compared in the same way. A change in this ratio implied a change in membrane resistance during the course of the experiment. Those fibers in which either the current- or the voltage-trace ratio varied by more than 7% were rejected.

A typical average constant-voltage pulse and constant-current pulse are illustrated in Fig. 6*A* and 6*B*, respectively, where in both cases the top trace shows membrane current and the bottom membrane voltage. In each case the time constant was obtained from a least-squares regression line of the logarithms of the difference of the membrane current or membrane voltage from their final values in the time interval 200 to 600 msec.[3] In the constant-voltage pulse (Fig. 6*A*) the slow transient drop in membrane current corresponds to an increase in the effective membrane resistance which increases to approximately 2.0 times its "initial" (post-capacity transient) value. The time constant was about 340 msec. Although not very accentuated in the figure (the effect will be shown more clearly in a later

3 The lower bound of the time interval was chosen so as to ensure that the capacity transients had decayed completely. On the other hand, the higher was chosen to limit the range of the analysis for two reasons: (1) At the tail of an exponential any uncertainty in its final value or the presence of noise will be greatly magnified by taking logarithms. (2) If the experimental points of an exponential function had a linear-normal distribution a linear regression analysis on a semi-logarithmic plot of those points would only tend to be valid over a relatively small region.

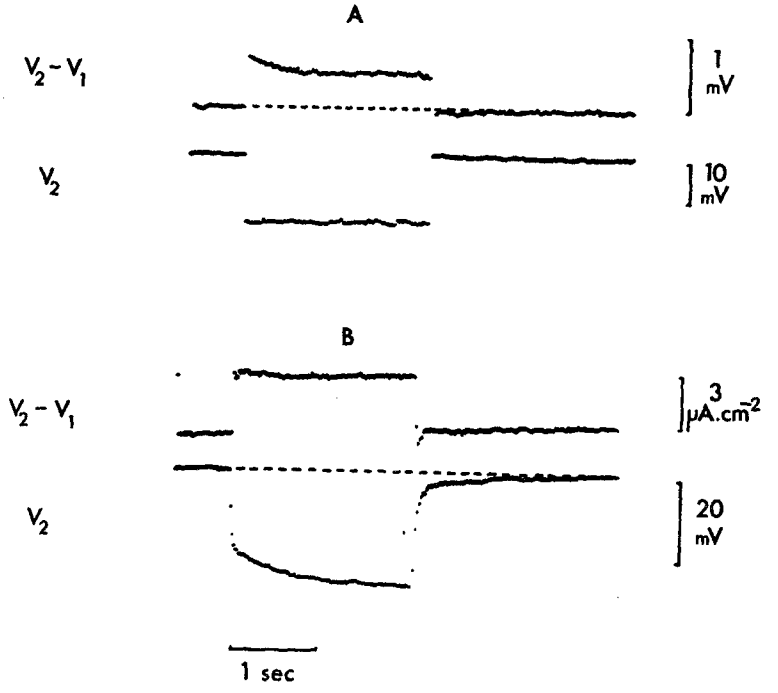

Fig. 6. (*A*) The average recorded from the Biomac oscilloscope of eight constant-voltage pulses for Fiber 9. These hyperpolarizing voltage pulses of 2-sec duration had a magnitude (V_1) of -15.6 mV. The top trace shows membrane current ($V_2 - V_1$) and the bottom trace membrane voltage (V_2). Note the considerable transient reduction in membrane current corresponding to a decrease in fiber conductance G_m. It should also be noted that for experimental reasons V_2 was controlled instead of V_1 but as can be seen, the change in V_1 during the pulse is only about 1 %. (*B*) The average record from the Biomac oscilloscope of eight constant-current pulses again for Fiber 9. These 2-sec duration hyperpolarizing current pulses had a magnitude of 3.4 $\mu A \cdot cm^{-2}$. The top trace again shows membrane current ($V_2 - V_1$) and the bottom membrane voltage (V_2; *see note* for Fig. 6*A*). Note the considerable decrease in voltage again corresponding to a decrease in fiber conductance G_m. The scales in both Fig. 6*A* and 6*B* are the same

figure, Fig. 7) at the termination of the pulse there is a small overshoot in the top trace indicating that the membrane current is now flowing in the opposite (outward depolarizing) direction. This overshoot decays slowly back to the base line voltage. In the constant-current pulse for the same fiber (Fig. 6*B*) there is now a slow transient increase in voltage. This however again corresponds to an increase in the effective membrane resistance which now increases to about 1.6 times its "initial" value. At the end of the current pulse there is a small "tail" of potential which decays slowly back to the base level. Such a "tail" corresponds again to an outward depolarizing current.

Table 3. A comparison of the experimental results[a] and the theoretical[a] predictions using the computed numerical analysis for the fibers of Table 2

Fiber no.	Constant-Voltage				Constant-Current			
	Experiment		Theory		Experiment		Theory	
	G_∞/G_0[d]	τ_{vc}	G_∞/G_0	τ_{vc}	G_∞/G_0	τ_{cc}	G_∞/G_0	τ_{cc}
5	0.59 ± 0.006	323 ± 11	0.58 ± 0.11	319 ± 53	0.65 ± 0.00	455 ± 15	0.64 ± 0.12	439 ± 68
7	0.60 ± 0.03	245 ± 54	0.70 ± 0.13	316 ± 53	0.71 ± 0.01	344 ± 14	0.71 ± 0.14	366 ± 57
9	0.59 ± 0.01	254 ± 20	0.58 ± 0.11	369 ± 62	0.68 ± 0.001	512 ± 18	0.64 ± 0.12	496 ± 77
14	0.51 ± 0.03	524 ± 73	0.61 ± 0.11	572 ± 96	0.71 ± 0.003	660 ± 33	0.70 ± 0.13	807 ± 126
18	0.55 ± 0.03	629 ± 143	0.60 ± 0.11	433 ± 72	0.71 ± 0.01	528 ± 30	0.66 ± 0.13	570 ± 89
19	0.53 ± 0.003	358 ± 12	0.58 ± 0.11	511 ± 85	0.75 ± 0.02	501 ± 85	0.67 ± 0.13	750 ± 117
Avg.[b]	0.56 ± 0.02	389 ± 63	0.61 ± 0.11	420 ± 70	0.70 ± 0.01	500 ± 42	0.67 ± 0.13	571 ± 89
Avg.[c] regr. coeff.	0.991 ± 0.002		1.0000 ± 0.000004		0.996 ± 0.001		0.9998 ± 0.0000	

[a] The fiber parameters used in the theoretical analyses were those discussed in the text, viz. $\rho'=0.0040$ ($\rho=0.0030$); $\sigma'=0.375$ ($\sigma=0.50$), so that $\bar{G}_L=1.5\times10^{-5}$; $\bar{D}_K=1.6\times10^{-5}$; $r_s=100\,\Omega\,\text{cm}^2$; $C_K=2.5$ mM·liter^{-1}. The conductance-voltage curve used was that given in Fig. 5, and the other parameters needed were obtained from Table 2. For rows 3 to 19 of the theoretical predictions the errors were obtained from Table 4, the errors in row 10 being the averages of those predicted errors in rows 3 to 9. In all other cases the errors shown are the SEM. In each case a regression analysis was used to calculate time constants and the ratio of final to initial conductance from the 200- to 600-msec part of each curve.

[b] The average and SEM in row 10 were obtained from rows 1 to 9 for experimental results.

[c] The average regression coefficient was that obtained from the regression analyses for the six fibers, and their closeness to 1.0000 in each case indicates that this 200- to 600-msec section of curve is well-approximated by a single exponential.

[d] G_∞/G_0, τ_{vc} and τ_{cc} represent the ratio of final-to-initial conductances, the voltage-clamp time constant and current-clamp time constant, respectively. The experimental results, obtained from regression analyses on enlarged and "smoothed" curves, were in every case the averages of two sets of measurements except in the voltage-clamp data of Fiber 5 where they were the average of four sets.

The measured and evaluated fiber parameters for the fibers used are given by Table 2. For the purposes of averaging fiber parameters, averages of a (μm) and R_m (KΩ cm) were obtained, and $\bar{G}_W$ and R_{sm} calculated from these averaged values. The magnitudes and time-constants of the slow conductance changes are given in Table 3. As far as the average for the six fibers is concerned the overall membrane conductance falls to 56% of its initial value (resistance increases to 179%) during voltage clamping and to 70% of its initial value (resistance increases to 143%) during current clamping.

The time-constant of these slow conductance changes or "creep" during such constant-current pulses is almost invariably longer (average is 500 ± 42 msec) than the time constant during constant-voltage pulses (average is 389 ± 63 msec).[4]

Justification of Parameters Used for Theoretical Analysis

As already mentioned, to calculate muscle fiber radius a conductivity of the TTS, $\bar{G}_W$, and surface membrane resistance R_{sm} it was necessary to know the internal resistivity of the fiber and the conductance of the TTS relative to the total "membrane conductance". The value of the internal resistivity of frog muscle fibers was taken from the measurements of Nakajima and Hodgkin (1970) who found an internal conductivity G_i of 5.91 ± 0.13 mmho·cm at 20 °C, which then corresponds to an internal resistivity of 169 ± 3.7 Ω cm. The value of the conductance fraction of the TTS, f_T, was taken from the measurements of Eisenberg and Gage (1969). They compared membrane conductance at high and low pH for intact fibers and for fibers with transverse tubular systems disrupted by glycerol treatment. They showed an average conductance of the surface membrane of 28 μmho·cm^{-2} compared to 55 μmho·cm^{-2} for the TTS giving a conductance fraction f_T of 0.66.

Following Adrian *et al.* (1969), G_L, the conductivity of the tubular lumen was considered to have a conductivity of 10^{-2} mho·cm^{-1} slightly less than the conductivity of Ringer's solution at 20 °C. They also showed that a variety of different tubular arrays each produced a network factor $\sigma = 0.5$, and so this value was used in this paper.

As far as the volume fraction of the tubular system was concerned the estimation of Peachey (1965), based on electron-micrographic studies, of 0.3% was chosen for the volume fraction of the transverse tubular system alone. The effect of the longitudinal branching of the tubular system was also taken into account. Peachey and Schild (1968) showed that longitudinal

4 The time constants τ_{vc} and τ_{cc} would be expected to differ for the following reasons. The current across the walls of the TTS is determined by the difference between E_K and the wall p.d. During a constant-voltage pulse only E_K is changing significantly, and the time constant of the change in current is set by this change in E_K directly. However, during a constant-current pulse, because the current through the surface membrane now increases as that in the TTS decreases, so the wall p.d., which is set by the current across the surface membrane, and E_K both increase. The effect of these two components being transient is to further increase the overall time-constant. The smaller the surface membrane resistance the less the TTS affects the current going through the surface membrane and the closer the overall time-constant (and change in conductance) tends towards the constant-voltage values.

branching should increase the volume fraction of the tubular system by about 30%. The volume fraction of the whole tubular system was then taken as 0.4%. As already mentioned on pp. 258 and 259 and the two different volume fractions were taken into account by increasing ρ to 0.0040 and decreasing σ by 75% to 0.375 so that $\sigma\rho$ still remained equal to 1.5×10^{-3}.

It seems likely (Peachey & Adrian, 1973) that the TTS has an access resistance and a separate investigation (Adrian, *unpublished*) has suggested a value of 100 Ω cm^2.

Now K^+ depletion in the tubular system will be concurrently accompanied by an increase in Na^+ and a decrease in SO_4^{2-} ions so that actual inter-diffusion of the whole system would be expected to be some mean of D_K, D_{Na} and $D_{SO_4^{2-}}$. However, it is known that for coupled inter-diffusion of two ion species in the presence of a third (counter-ion) species the species whose concentration is low dominates the inter-diffusional flux (Lakshminarayanaiah, 1969) i.e. for K^+ and Na^+ in the presence of a third ion (e.g. SO_4^{2-}) provided $C_K \ll C_{Na}$ then $D_{Na-K} \approx D_K$. This is obvious because for the same change in concentration for the two species the change relative to the absolute concentration is much greater for the species with the lower absolute concentration. Now the analysis and experiments discussed by Lakshminarayanaiah assumed that the counter ion concentration was constant but presumably the principle would still tend to apply even if this was not the case. The ionic diffusion constant D_K for K^+ in a free salt solution of about 100 mM·liter^{-1} concentration at 20 °C was estimated with some minor extrapolation from the tables of Robinson and Stokes (1965) to be 1.6×10^{-5} cm^2·sec^{-1} and this was the value chosen for K^+ diffusion in the tubular system.

It was also assumed that the access resistance was just due to geometry factors so that the diffusional access resistance h could be calculated [Eq. (29)] from the electrical access resistance r_s and the electrical conductivity of the tubular lumen G_L and the K^+ diffusion constant D_K. For two of the parameters, G_L, the conductivity, and D_K, the K^+ diffusion coefficient, in the tubular lumen, the free-solution values were chosen. It has been suggested (Schneider, 1970), from an analysis to evaluate the equivalent electrical circuit of a muscle fiber, that the internal resistivity of the tubular lumen is about 300 Ω cm. This is equivalent to reducing G_L to about one-third of its free-solution value. The analysis however did not consider the possibility of an access resistance in series with the tubular lumen. The value of 100 Ω cm^2 in series with an average tubular resistance of about 83 Ω cm^2 for the fibers in this paper [$a/(4\bar{G}_L)$, *cf.* Adrian *et al.*, 1969] should be somewhat equivalent to the higher value of tubular lumen resistance without any access resistance (*see* Table 5 and pp. 281–282). With the inclusion of such an access resistance there seems to be no need to reduce either G_L or D_K below their free-solution values. Also, Almers (1972*b*) mentions a calculation (Almers and Barry, *unpublished calculation*) for the recovery of depletion, which in fact makes use of a modification of an earlier version of the numerical analysis presented in this paper, and uses a value of D_K reduced

to about one-third. This gives a reasonable reconstruction of his experimental curves. However, again no access resistance was used and the same comments apply as for G_L.

To calculate errors for the predicted theoretical curves discussed in the next section the following uncertainties in the various parameters of the average fiber were considered to be reasonable: $\Delta R_i/R_i = 3.7/169$; $\Delta \bar{G}_L/\bar{G}_L = 0.15/1.5$; $\Delta \rho/\rho = 0.02/0.40$; $\Delta r_s/r_s = 10/100$; $\Delta f_T/f_T = 10/66$; $\Delta D_K/D_K = 0.05/1.6$; $\Delta V_0/V_0 = 0.1/15.4$; $\Delta I/I = 0.2/3.1$.

Comparison of Theory and Experimental Results Together with Further Predictions

Using the fiber parameters of Table 2 and the tubular system parameters discussed in the last section, constant-voltage and constant-current pulses were computed using the numerical procedures described earlier. Figs. 7 and 8 show a comparison of such theoretically predicted curves with the experimental ones over the whole time course of both constant-voltage and constant-current pulses for a particular fiber (Fiber 5 in Tables 2 and 3). In

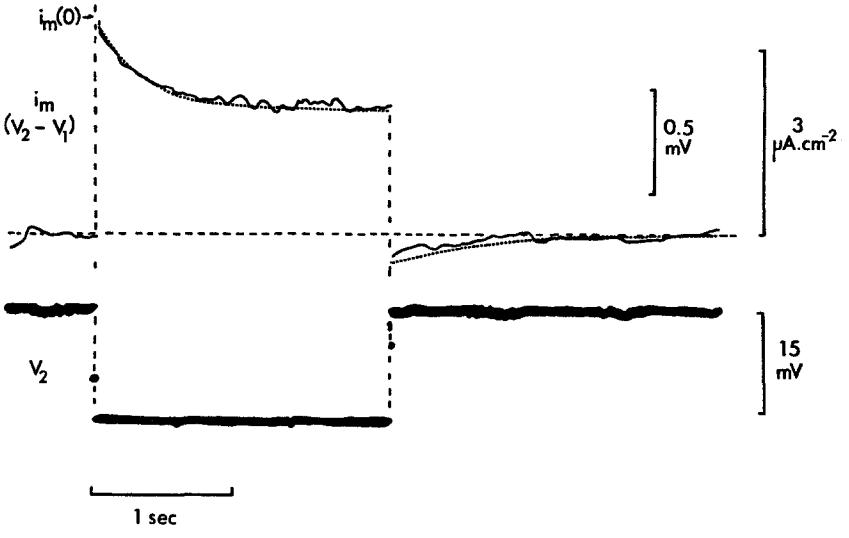

Fig. 7. Redrawn enlargements of the average from the Biomac oscilloscope of eight constant-voltage (hyperpolarizing) pulses of 2-sec duration for Fiber 5 (*cf.* Fig. 6 for Fiber 9). The amplitude of the top membrane current trace ($i_m = V_2 - V_1$) has also been doubled and for clarity only the center of the trace drawn in, whereas the bottom voltage (V_2; *see note* for Fig. 6*A*) trace has just simply been enlarged. The dashed curve is the curve predicted by the full numerical analysis of K^+ depletion in the tubules using the measured fiber parameters (Table 2) and TTS parameters discussed in the text. The arrow indicates the "initial" (excluding capacity transient) extrapolated value of the membrane current $i_m(0)$ as discussed in the text. Note the close agreement between theory and experiment for both the duration and turn-off of the pulse

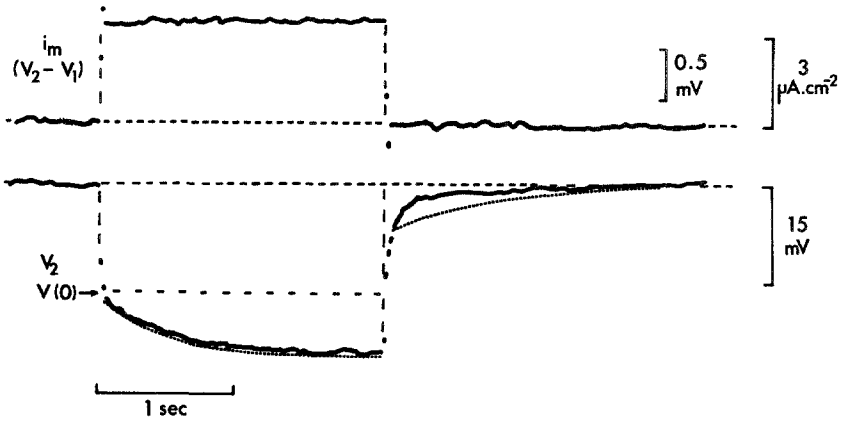

Fig. 8. Redrawn enlargements of the average from the Biomac oscilloscope of eight constant-current (hyperpolarizing) pulses of 2-sec duration for Fiber 5 (*cf.* Fig. 6*B* for Fiber 9). Although only the center of each trace has been drawn in for clarity this is in all other respects just a simple enlargement. Again the top trace is membrane current ($i_m = V_2 - V_1$) and the bottom membrane voltage (V_2; *see note* for Fig. 6*A*). The dashed curve is the curve predicted by the full numerical analysis of K^+ depletion in the tubules using the same parameters as for Fig. 7, and discussed in the text. The arrow indicates the "initial" (excluding capacity transient) extrapolated value of the membrane voltage $V(0)$ as discussed in the text. Note the close agreement between theory and experiment for the duration of the pulse. The divergence between predicted and observed voltage traces at the turn-off of the pulse is discussed in the text

both cases, of course, the "initial" values of the theoretical curves should have essentially the same values as those of the experimental curves since the former used the conductance parameters obtained experimentally. In practice, mainly to overcome uncertainties due to capacity transients, the two curves, experimental and theoretical, were scaled so as to have the same "initial" values extrapolated using the 200- to 600-msec part of each curve.

As shown in Fig. 7 during a constant-voltage pulse the theoretical curve lies reasonably close to the experimental one. During the duration of the pulse the experimental membrane current drops as expected with almost exactly the same time course and final values as the theoretically predicted current (*see* Table 3) corresponding to a transient decrease in measured membrane conductance. Similarly, at the termination of the pulse there is, as predicted, a small transient reversal of the membrane current. For the duration of the constant-current pulse (Fig. 8) there is also very good agreement between the experimental and theoretical curves with voltage creep again corresponding to a transient decrease in the measured fiber conductance. However, when the current pulse is terminated the theory

predicts a somewhat larger decay tail than is observed experimentally. The discrepancy between the two curves may be due to a decrease in that component of the K^+ conductance independent of $V-E_K$ as a result of a drop in the tubular K^+ concentration and possibly also a decrease in the K^+ transport number in the membrane for currents in the high resistance direction as suggested on p. 253. Such a K^+ dependence was not taken into account in the theoretical analysis and should be maximal at the *turn-off* of the *constant-current* pulses since experimentally the change in membrane potential and the drop in K^+ concentration is greater then than at the turn-off of constant-voltage pulses. The larger drop in tubular K^+ concentration would then cause a greater change in E_K and therefore a greater resistance for outward currents. In addition, a greater drop in tubular K^+ might result in a further drop in the outward conductance. Thus, both effects should cause smaller outward currents following *constant-current* pulses.

As already mentioned, measurements were made on a number of fibers. The transient "creep" parts of the current and voltage curves in each case were analyzed in terms of time constants and the ratio of final-to-initial conductances. First of all, enlargements were made of the Biomac oscilloscope film recordings. Then points were measured from a "smoothed" curve drawn through the resultant trace. The logarithms of points from this part of the curve over the range from 200 to 600 msec and the steady-state values were then fitted by computer to a linear regression line using a least-squares analysis. The initial extrapolated value of the conductance and the exponential time-constant of the curve were thus evaluated. As Table 3 indicates, the average for both constant-voltage and constant-current pulses was better than 0.99 indicating that at least over this section of the curve the experimental transients fitted a single exponential well. Theoretical curves were computed for all the fibers using the parameters given in Table 2 together with the conductance-voltage curve of Fig. 5 and the other TTS parameters already mentioned. These predicted curves were analyzed by regression analysis over the range of 200 to 600 msec in the same way as the experimental curves, and a comparison between the theoretical predictions and experimental observations is given in Table 3. The experimental values were in all cases the average of two sets of measurements from the enlarged tracings except for the constant-voltage results of Fiber 5 where four sets were used. The experimental values in every case represent the mean $\pm$SEM. Errors for the predicted theoretical curves were computed using the total relative errors listed in Table 4 and the average error represents the mean of the predicted errors for the six fibers.

Table 4. An estimation of the possible relative errors expected[a] in the numerical analysis computations as a result of parameter uncertainties

Possible relative parameter errors	Voltage-clamp		Current-clamp	
	$\Delta(G_\infty/G_0)/(G_\infty/G_0)$	$\Delta\tau_{vc}/\tau_{vc}$	$\Delta(G_\infty/G_0)/(G_\infty/G_0)$	$\Delta\tau_{cc}/\tau_{cc}$
$\Delta R_i/R_i$ =3.7/169	+0.003	+0.013	+0.002	+0.010
$\Delta G_L/G_L$ =0.15/1.5	−0.018	+0.014	−0.014	+0.023
$\Delta\rho/\rho$ =0.0002/0.004	+0.003	+0.035	+0.006	+0.042
$\Delta r_s/r_s$ =10/100	−0.016	+0.016	−0.014	+0.023
$\Delta f_T/f_T$ =10/66	−0.132	−0.077	−0.136	+0.016
$\Delta D_K/D_K$ =0.05/1.6	+0.008	−0.009	+0.011	−0.022
$\Delta V/V$ =0.1/15.4	−0.002	−0.003	−	−
$\Delta I/I$ =0.2/3.1	−	−	−0.008	−0.020
Total relative error[b]	0.182	0.167	0.191	0.156

[a] These relative errors were computed using the model fiber parameters similar to the parameters of the average fiber of Table 3 and should apply reasonably well for each of the fibers in that table. The sign indicates whether an increase in the relative parameter given in column 1 will cause an increase (+) or a decrease (−) in the relative conductance ratio or time-constant.

[b] The total relative error in row 11 is the sum of the absolute magnitudes of the relative errors in rows 3 to 10.

On the one hand, as Table 3 indicates for the individual fibers, two sets of the experimental and theoretical values of the constant-voltage time-constants (for Fibers 9 and 19) and one of the current time-constants (for Fiber 19) do lie outside of the estimated errors. These discrepancies may be due to errors in recording (as a result of noise, especially in recording membrane current, *cf.* Figs. 6, 7 and 8) and "smoothing" of the curves or could be real and due to errors in estimating the membrane or TTS parameters.

On the other hand, for the rest of the results in Table 3, for the individual fibers, there is good agreement between the experimental results and the theoretical predictions within the given estimated errors. In addition, there is good agreement, well within the estimated errors between experimental results and theoretical predictions, for the averages of conductance changes and both the constant-voltage and constant-current time-constants.

The average regression coefficients listed in Table 3 for the theoretical predictions indicate that, in accordance with the experimental results, over the range from 200 to 600 msec the curve is fitted well by a single exponential. Actually a semi-logarithmic plot of predicted constant-current and

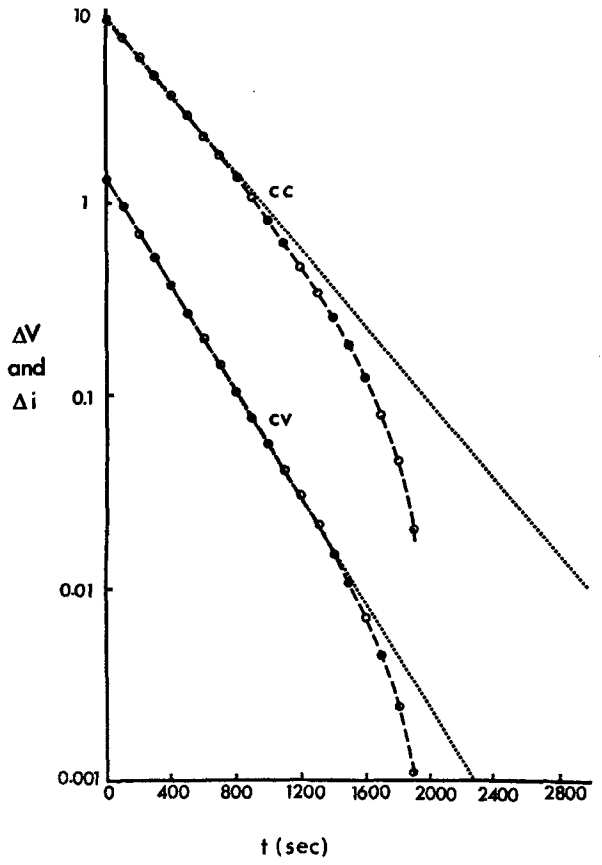

Fig. 9. The changes in voltage ΔV and current Δi with respect to the steady-state (2.0 sec) values for constant-current (*cc*) and constant-voltage (*cv*) pulses with the parameters of Fiber 5. These values were predicted using the full computed numerical analysis and the results plotted on a logarithmic scale. It may thus be seen that the constant-voltage curve may be approximated by a single exponential over the range from 0 to 1,400 msec and the constant-current curve over the range from about 100 to 800 msec

constant-voltage curves in Fig. 9 indicates that the constant voltage curve does fit a single exponential closely over the range from 0 to 1,400 msec and the constant-current curve one over the range from 100 to 800 msec.

Computations were also done to investigate the effect of reducing the electrical access resistance r_s from 100 $\Omega\,cm^2$ (and correspondingly the diffusional access resistance h) to zero while leaving the total radial resistance $[r_s + a/4\bar{G}_L, cf.$ Eq. (9)] unaltered. This was done by reducing $\bar{G}_L$ from 1.5×10^{-5} to 0.642×10^{-5} mho $\cdot$ cm^{-1} and D_K from 1.6×10^{-5} to 0.685×10^{-5} cm$^2 \cdot$ sec^{-1}. The computations used the parameters of Fiber 5 and the results are shown in Table 5. It can be seen that with these constraints such a reduction in the

Table 5. The effect of reducing access resistance on the predicted slow conductance changes for Fiber 5. These were computed in both cases with the same total radial resistance and are compared with the values obtained experimentally

Parameters[a] of conductance changes	Experimental values	Predicted values[b]	
		$r_s = 100\ \Omega\ \text{cm}^2$	$r_s = 0$[c]
$G_\infty/G_0]_{vc}$	0.59 ± 0.01	0.58	0.64
τ_{vc}	323 ± 11	319	336
$G_\infty/G_0]_{cc}$	0.65 ± 0.00	0.64	0.70
τ_{cc}	455 ± 15	439	420

[a] $G_\infty/G_0]_{vc}$ and $G_\infty/G_0]_{cc}$ represent the ratio of final (actually, $t = 2$ sec)-to-initial conductances for voltage-clamp and current-clamp pulses, respectively. Similarly, τ_{vc} and τ_{cc} represent the voltage-clamp and current-clamp time-constants in msec calculated from a regression analysis over the 200- to 600-msec parts of each curve.

[b] The numerical analyses used the parameters of Fiber 5 (*see* Table 2) together with the TTS parameters discussed in the text (*see also* legend to Table 3) except where indicated below.

[c] To keep the total radial resistance the same, when r_s was reduced to zero, $\bar{G}_L$ was reduced from 1.5×10^{-5} to 0.642×10^{-5} mho·cm^{-1} and D_K from 1.6×10^{-5} to 0.685×10^{-5} cm^2·sec^{-1}.

access resistance did not make a large difference to the magnitudes and time constants of the conductance changes. In fact, the time constants were hardly affected at all although the magnitudes of the final conductance changes were reduced by about 10% so that the predicted conductance curves for $r_s = 0$ were not as good a fit as those with $r_s = 100\ \Omega\ \text{cm}^2$.

Furthermore, it has been recognized that these "creep" effects only seem to occur during hyperpolarizing pulses. This at first seems unexpected since it would seem that depolarizing current should also tend to increase the K^+ concentration in the tubules in opposition to the electrical p.d. thus reducing K^+ movement across the tubular wall and hence again slowly decreasing the measured conductance of the fiber. This might be expected to result in time-dependent current or voltage curves which are mirror-images of those obtained for hyperpolarizing pulses, though perhaps somewhat reduced in magnitude for larger depolarizations. This is in fact what the theory predicts for a tubular conductance which is independent of $(V - E_K)$. However, if the actual experimental relationship for potassium conductance as a function of voltage obtained by Adrian and Freygang (1962) is used (*see* Fig. 5 and p. 269) then Figs. 10 and 11 show that whereas there should be a significant concentration enhancement of K^+ (from 2.5 mM to 3.0 mM, Fig. 10), for a *depolarizing* pulse of 15 mV the current

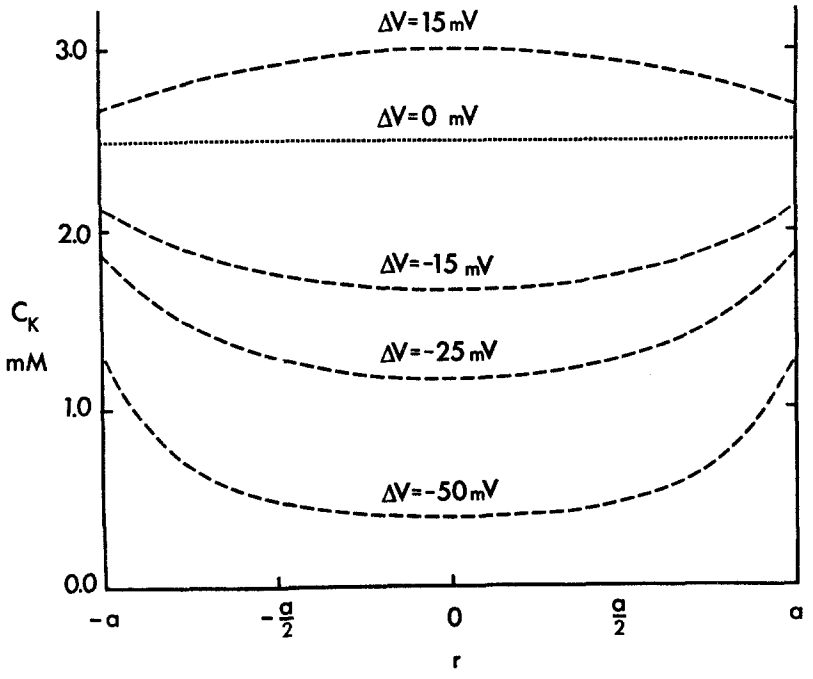

Fig. 10. Predicted K^+ concentration profiles within the tubular system of a muscle fiber (radius $=a$) at the beginning ($\Delta V=0$) and end of constant-voltage pulses of various amplitudes ΔV. The initial and external bathing solution concentration of K^+, C_K, was taken as 2.5 mM·liter^{-1}. The model fiber parameters (Table 2) together with the TTS parameters and the conductance-voltage curve discussed in the text (*see also* Fig. 5) were used in a full numerical analysis. It should be noted that a depolarizing pulse of 15 mV does produce a significant increase in concentration at the center of the fiber. Note also the effect of the access resistance, which allows the K^+ concentration at $r=a$ to drop below the concentration in the external solution

(Fig. 11) only drops about 6% with a time constant of 1.0 sec and would be almost impossible to observe especially with other time-dependent effects that seem to take place when a membrane is depolarized. However, Almers (1972*a*) has observed a small positive shift in the zero-current potential (i.e., the overall K^+ equilibrium potential) following a 10-mV depolarizing pulse as would be expected from an accumulation of K^+ in the TTS.

On the other hand, if a muscle fiber is placed in a Rb_2SO_4 Ringer's solution without Cl^- the membrane conductance should be approximately constant with applied voltage (Adrian, 1964) and hence, as mentioned earlier, the responses of depolarizing pulses should tend to mirror those of hyperpolarizing ones. In such solutions, at least for small voltage pulses, the approximate analytical solutions should now be reasonably accurate and

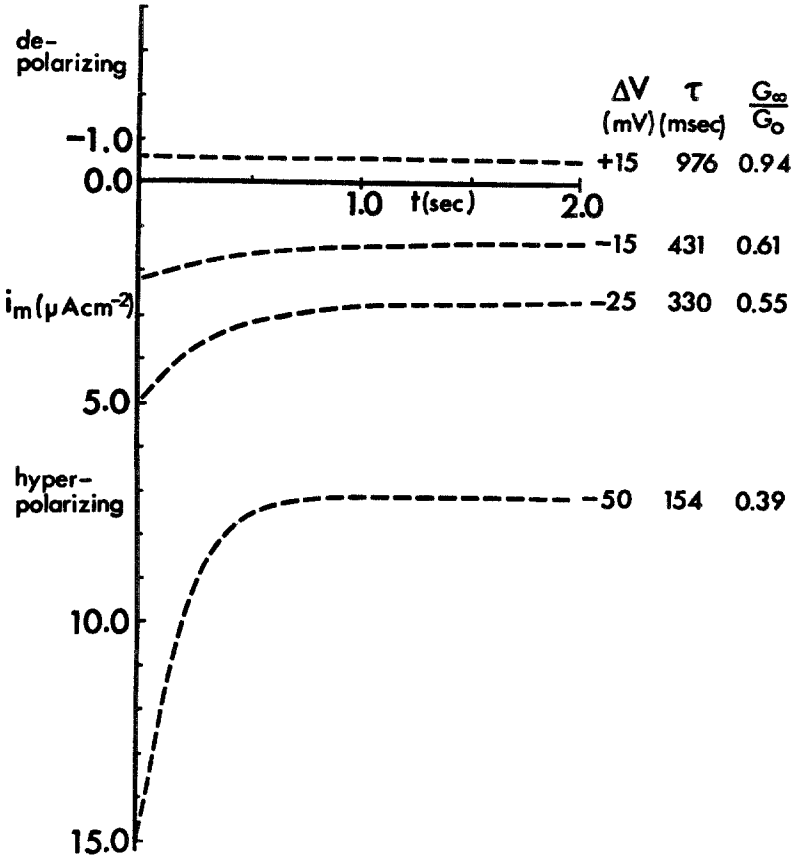

Fig. 11. Predicted time-dependent membrane currents i_m just due to K^+ depletion during a series of constant-voltage pulses of different amplitudes ΔV. These calculations used the same parameters (model fiber) and techniques as for Fig. 10. It should be noted that in spite of the considerable enhancement of K^+ in the center of the fiber (Fig. 10) there is almost no discernable current "creep" during the 15-mV depolarizing pulse

at higher voltages (pulses of about 20 mV or so) should at least give reliable qualitative predictions. Unfortunately, although the conductance is now linear, the Rb^+ currents are now 5 to 10 times smaller than the equivalent K^+ currents for the same hyperpolarizing voltage (Adrian, 1964). If the time- and voltage-dependent permeability component still becomes significant for Rb^+ at voltages of approximately -120 mV (Almers 1970*a*, *b*) then depletion effects by themselves will be correspondingly smaller and harder to detect.

Even for K^+ solutions, however, the constant conductance model will be useful for qualitatively predicting the differences between voltage-clamp

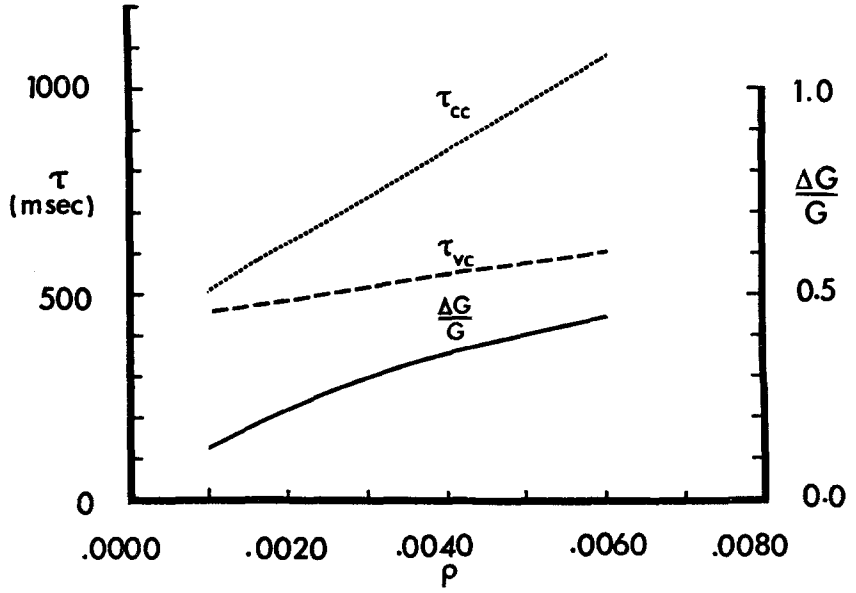

Fig. 12. Predicted constant-current time constants τ_{cc}, constant-voltage time constants τ_{vc} and relative change in conductance $\Delta G/G$ as a function of the volume fraction of the TTS (transverse+longitudinal tubules), ρ. This used the model fiber parameters (Table 2) and published TTS parameters discussed in the text, assumed that G_L and G_W were constant and hence the curves are in large measure responding to changes in $\bar{G}_L$ and $\bar{G}_W$. The approximate mathematical analysis was used and hence it was further assumed that conductance was independent of voltage. The predictions are therefore most applicable quantitatively to a fiber in a SO_4 Ringer's solution only experiencing very small changes in voltage

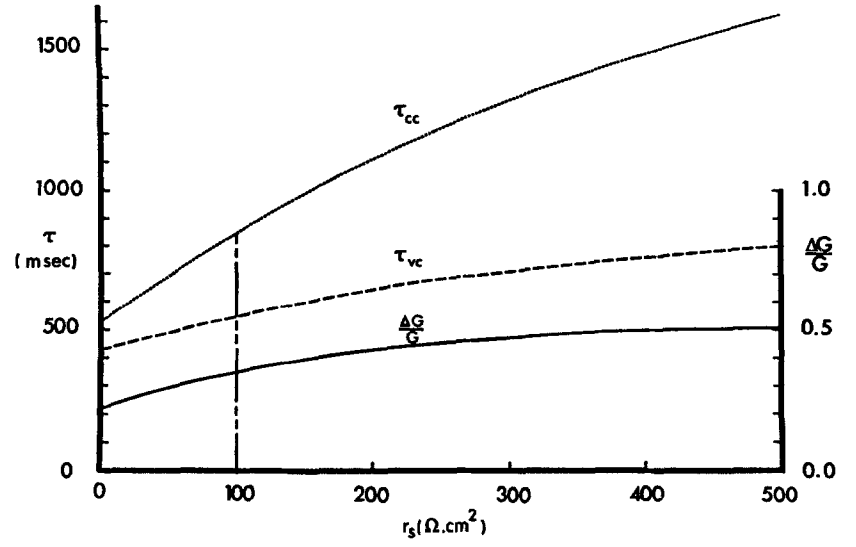

Fig. 13. Constant-current and constant-voltage time-constants (τ_{cc} and τ_{vc}, respectively) and relative conductance change $\Delta G/G$ as a function of access resistance r_s of the TTS predicted from the time-dependent mathematical analysis. $\rho = 0.0040$ and the other parameters are the same as those used for Fig. 12. The vertical line indicates the values at $r_s = 100\ \Omega\ cm^2$. Again the analysis is most quantitatively applicable to a fiber in a SO_4 Ringer's solution only experiencing very small changes in voltage

and current-clamp time-constants. These differences may then become a very useful tool for monitoring changes in access resistance and tubular volume. Fig. 12 shows that as tubular volume increases, voltage-clamp and current-clamp time-constants together with the relative conductance change $\Delta G/G(0)$ all increase. Similarly, Fig. 13 indicates that both time-constants and the relative conductance change all increase as the access resistance is increased.

Discussion

This paper has shown that from a consideration of physico-chemical principles, in particular transport number effects, together with the generally accepted geometry of the tubular system of muscle fibers that a hyperpolarizing voltage or current pulse should cause a depletion of K^+ in the tubular system of muscle and thus (at least for small voltage changes) produce transient increases in resistance of the same magnitude and time course as those observed experimentally.

In particular, the experiments on muscle fibers under constant-voltage and constant-current pulse conditions were compared with the theoretical predictions for conductance "creep" resulting from tubular K^+ depletion and estimated using experimentally measured parameters together with the generally accepted geometry factors for the tubular system. For the small voltage changes used (15 mV initially and in the case of constant-current pulses increasing to about 30 mV at the end of the pulse) there was good agreement within estimated errors between experiment and theory for almost all of the results for the individual fibers and for the average results for both relative conductance changes and time-constants. However there were some discrepancies during the turn-off of the constant-current pulses. As already mentioned on p. 279 this was probably due to a decrease in that component of the K^+ conductance independent of $V-E_K$ but dependent on tubular K^+ concentration and possibly also a decrease in the K^+ transport number in the membrane for currents in the high resistance direction. The former effect would be expected to cause smaller outward currents following *constant-current* pulses. In fact, Almers (1972*a*) has shown that at higher K^+ concentrations a K^+ concentration dependence of the tubular K^+ conductance satisfactorily explains the rather complex biphasic current recovery response seen in a series of double voltage-clamp pulse experiments.

Both for individual fibers and for the average of the six fibers the agreement between theory and experiment provided further validation of the present knowledge of the tubular system in muscle and provided further

proof that at least for these low voltages current and voltage creep could be wholly explained in terms of potassium depletion in the tubular system. The magnitude of the applied voltages has been stressed because, as already mentioned, Almers (1972*a*, *b*) has shown that at higher voltages (>20 mV) these slow conductance changes seem to involve another component with a high Q_{10} of the same order as that seen during a membrane action potential.

This explanation of the phenomenon of conductance "creep" in muscle for small changes in membrane voltage suggests the possibility that many other similar transient electrical phenomena in biological systems may well be explainable in terms of relatively simple (at least in principle) physicochemical processes such as transport number effects and diffusional effects taking place in unstirred regions near membranes rather than as an extra complexity in the conductances of the individual membranes themselves. It also provides a very useful tool for obtaining additional information about the transverse tubular system of muscle fibers. For example, a recording of conductance "creep" in muscle fibers with voltage-clamp and current-clamp pulses could provide a means of monitoring tubular volume and access resistance. If this was done during the process of detubulation of muscle fibers in glycerol solutions it could provide very valuable information on the actual mechanism of detubulation. Also, a measurement of the magnitude of "creep" could be used as a diagnostic tool for the determination of the fraction of transverse tubules left after detubulation.

The authors would like to thank Dr. R. S. Eisenberg for stimulating discussion and Drs. W. Almers and P. W. Gage for their helpful critical reading of the manuscript, and W. Smith for technical assistance. P. H. B. would also like to thank the Wellcome Trust for a post-doctoral fellowship during the first part of the project at the University of Cambridge and the Queen Elizabeth Fellowship Committee for a post-doctoral fellowship during its final stages at the University of New South Wales.

Appendix A

Effective Parameters for an Equivalent Disc Representing the TTS *in Muscle Fibers*

The basic parameters of the actual T-system of a muscle fiber have been defined in the text and in the accompanying symbol list.

Consider a unit surface area of fiber to incorporate n equivalent T-system discs, each of thickness d cm. The total surface area A of both sides of these

equivalent discs will be given by:

$$A=2n\pi a^2 \tag{A.1}$$

and volume of these equivalent discs V by:

$$V=n\pi a^2 d. \tag{A.2}$$

Now ρ is the volume fraction of the TTS and ξ is the volume-to-surface ratio of the TTS. Hence the *actual surface area of the* TTS, A_t referred to unit area of fiber surface, will be given by:

$$A_t=\frac{\rho}{\xi}\frac{a}{2} \tag{A.3}$$

since the surface area of unit volume of fiber is $2/a$ cm^2. Now the following relationships should apply between the actual T-system parameters and the effective parameters of an equivalent disc. There is in fact no loss in generality in considering just *one* equivalent disc (i.e., $n=1$), and in fact it is rather more convenient for both diagrams and discussion to do so. Thus: (*i*) The total conductance of the equivalent disc should be the same as the total conductance of the actual TTS. If G'_W is the effective conductance across both sides of an equivalent disc/cm^2 of the surface area of one side then:

$$G'_W 2\pi a^2=\frac{\rho}{\xi}\cdot\frac{a}{2}\cdot G_W \tag{A.4}$$

or

$$G'_W=\frac{\frac{\rho}{\xi}\cdot G_W}{4\pi a}=\frac{\bar{G}_W}{4\pi a} \tag{A.5}$$

where, by definition,

$$\bar{G}_W=\frac{\rho}{\xi}G_W \tag{A.6}$$

is the conductance of the TTS per unit volume of fiber. (*ii*) Similarly, the volume of the equivalent disc should be the same as the volume of the actual TTS. Since the volume of the TTS/unit area of fiber surface V_t is given by:

$$V_t=\rho a/2. \tag{A.7}$$

Hence,

$$\pi a^2 d = \rho a/2 \tag{A.8}$$

or

$$d = \frac{\rho}{2\pi a}. \tag{A.9}$$

(*iii*) The diffusion constant of K^+ in the TTS, D_K, and the specific conductivity of the TTS lumen G_L in a radial direction will not be affected by the width of the equivalent disc but will be affected by a geometry factor since the TTS is in reality a mesh of tubules. Adrian *et al.* (1969) have shown that such effective parameters should be related to the actual tubular lumen parameters by a geometry or network factor σ. In fact, they have shown that for a number of different types of tubular mesh the same factor σ of 0.5 still applies. This means that the effective diffusion coefficient D_K and lumen conductivity G'_L for the equivalent disc should be related to the actual values of D_K and G_L for the tubular lumen by:

$$D'_K = \sigma D_K \tag{A.10}$$

and

$$G'_L = \sigma G_L. \tag{A.11}$$

Appendix B

The Relationship Between Conductances under Constant-Voltage and Constant-Current Conditions as the Surface Membrane Resistance Decreases to Zero

From Eqs. (42) and (43) the total voltage-clamp conductance $G_{vm}(t)$ is given by:

$$G_{vm}(t) = G_m(\infty) + G(\alpha, \omega, t) + \sum_{m=1}^{\infty} G(i\alpha_m, \omega, t) \tag{B.1}$$

where by definition:

$$G(\alpha, \omega, t) = -\frac{4\phi \bar{G}_W \alpha^2 e^{-(\phi-\alpha^2)t}}{(\phi-\alpha^2) M(\alpha, \omega)} \tag{B.2}$$

and

$$G(i\alpha_m, \omega, t) = -\frac{4\phi \bar{G}_W \alpha_m^2 e^{-(\phi+\alpha_m^2)t}}{(\phi+\alpha_m^2) M(i\alpha_m, \omega)} \tag{B.3}$$

where $M(\alpha, \omega)$ and $M(i\alpha_m, \omega)$ are given by the $M(\alpha)$ and $M(i\alpha_m)$ of Eq. (46) and $G_m(\infty)$ by Eq. (43).

Now in the current-clamp situation, from Eqs. (60) and (61), the total resistance $R_{cm}(t)$ of the membrane is given by:

$$R_{cm}(t)=R_m(\infty)-R_{sm}^2\left\{G(\alpha, \omega', t)+\sum_{m=1}^{\infty} G(i\alpha_m, \omega', t)\right\} \tag{B.4}$$

where the $G(\alpha, \omega', t)$ and $G(i\alpha_m, \omega', t)$ have the same definition as that given in Eqs. (B.2) and (B.3) except that $\omega'(=\bar{G}_W(r_s+R_{sm}))$ replaces $\omega(=\bar{G}_W r_s)$ and where it has already been shown that the inverse of the current-clamp infinite resistance $1/R_m(\infty)$ is identical to the voltage-clamp infinite conductance $G_m(\infty)$. Thus, the current-clamp membrane conductance $G_{cm}(t)$, will be given by the inverse of $R_{cm}(t)$ as:

$$G_{cm}(t)=\frac{1}{\dfrac{1}{G_m(\infty)}-R_{sm}^2\left\{G(\alpha, \omega', t)+\sum_{m=1}^{\infty} G(i\alpha_m, \omega', t)\right\}}. \tag{B.5}$$

Now as $R_{sm}\to 0$, or as $R_{sm}/R_T \ll 1$, where R_T is the resistance of the transverse tubular system and does not include the surface membrane resistance, then by expansion it is easily shown from Eq. (B.5) that:

$$G_{cm}(t)\sim G_m(\infty)+G(\alpha, \omega, t)+\sum_{m=1}^{\infty} G(i\alpha_m, \omega, t) \tag{B.6}$$

which is the same as Eq. (B.1). This indicates as expected intuitively that a very small surface membrane resistance during constant-current conditions tends to have the same effect, as far as resistance and conductance changes are concerned, as applying constant-voltage pulses.

References

Abramowitz, M., Stegun, I. A. 1965. Handbook of Mathematical Functions. Dover Publications Inc., New York

Adrian, R. H. 1964. The rubidium and potassium permeability of frog muscle membrane. *J. Physiol.* **175**:134

Adrian, R. H., Chandler, W. K., Hodgkin, A. L. 1969. The kinetics of mechanical activation in frog muscle. *J. Physiol.* **204**:207

Adrian, R. H., Chandler, W. K., Hodgkin, A. L. 1970*a*. Voltage clamp experiments in striated muscle fibres. *J. Physiol.* **208**:607

Adrian, R. H., Chandler, W. K., Hodgkin, A. L., 1970*b*. Slow changes in potassium permeability in skeletal muscle. *J. Physiol.* **208**:645

Adrian, R. H., Freygang, W. H. 1962. The potassium and chloride conductance of frog muscle membrane. *J. Physiol.* **163**:61

Almers, W. 1972*a*. Potassium conductance changes in skeletal muscle and the potassium concentration in the transverse tubules. *J. Physiol.* **225**:33

Almers, W. 1972*b*. The decline of potassium permeability during extreme hyperpolarisation in frog skeletal muscle. *J. Physiol.* **225**:57

Barry, P. H., Hope, A. B. 1969*a*. Electroosmosis in membranes: Effects of unstirred-layers and transport numbers. I. Theory. *Biophys. J.* **9**:700

Barry, P. H., Hope, A. B. 1969*b*. Electroosmosis in membranes: Effects of unstirred-layers and transport numbers. II. Experimental. *Biophys. J.* **9**:729

Dewhurst, D. J. 1960. Concentration polarisation in plane membrane-solution systems. *Trans. Faraday Soc.* **56**:599

Eisenberg, B., Eisenberg, R. S. 1968. Selective disruption of the sarcotubular system in frog sartorius muscle. *J. Cell Biol.* **39**:451

Eisenberg, R. S., Gage, P. W. 1969. Ionic conductances of the surface and transverse tubular membranes of frog sartorius fibers. *J. Gen. Physiol.* **53**:279

Endo, M. 1966. The entry of fluorescent dyes into the sarcotubular system of the frog muscle. *J. Physiol.* **185**:224

Gage, P. W., Eisenberg, R. S. 1969. Action potentials, after potentials, and excitation-contraction coupling in frog sartorius fibers without transverse tubules. *J. Gen. Physiol.* **53**:298

Horowicz, P., Gage, P. W., Eisenberg, R. S. 1968. The role of the electrochemical gradient in determining potassium fluxes in frog striated muscle. *J. Gen. Physiol.* **51**:193s

Huxley, H. E. 1964. Evidence for continuity between the central elements of the triads and the extracellular space in frog sartorius muscle. *Nature* **202**:1067

Katz, B. 1949. Les constantes électriques de la membrane du muscle. *Arch. Sci. Physiol.* **3**:285

Lakshminarayanaiah, N. 1969. Transport Phenomena in Membranes. Academic Press Inc., New York

McCracken, D. D. 1965. A Guide to Fortran IV Programming. John Wiley and Sons, Inc., New York.

Nakajima, S., Hodgkin, A. L. 1970. Effect of diameter on the electrical constants of frog skeletal muscle. *Nature* **227**:1053

Page, S. G. 1964. The organisation of the sarcoplasmic reticulum in frog muscle. *J. Physiol.* **175**:10 P

Peachey, L. D. 1965. The sarcoplasmic reticulum and the transverse tubules of the frog sartorius. *J. Cell Biol.* **25**:209

Peachey, L. D., Adrian, R. H. 1973. Electrical properties of the transverse tubular system. *In:* Structure and Function of Muscle. G. H. Bourne, editor. 2nd Ed., Vol. 3. Academic Press Inc., New York

Peachey, L. D., Schild, R. F. 1968. The distribution of the T-system along the sarcomeres of frog and toad sartorius muscles. *J. Physiol.* **194**:249

Ralston, A. 1965. A First Course in Numerical Analysis. McGraw-Hill Book Co., Inc., New York

Robinson, R. A., Stokes, R. H. 1965. Electrolyte Solutions. Butterworths, London

Schaefer, H., Schölmerich, P., Haass, P. 1939. Der Elektrotonus und die Erregungsgesetze des Muskels. *Pflug. Arch. Ges. Physiol.* **241**:310

Schneider, M. F. 1970. Linear electrical properties of the transverse tubules and surface membrane of skeletal muscle fibers. *J. Gen. Physiol.* **56**:640

Wedner, H. J., Diamond, J. M. 1969. Contributions of unstirred-layer effects to apparent electrokinetic phenomena in the gall-bladder. *J. Membrane Biol.* **1**:92